5-2019

Pressure Loss Coefficients for Large Mitered Elbows with Diameters Ranging from 36-inches to 144-inches

Hayden J. Coombs
Utah State University

PRESSURE LOSS COEFFICIENTS FOR LARGE MITERED ELBOWS WITH DIAMETERS RANGING FROM 36-INCHES to 144-INCHES

by

Hayden J. Coombs

A thesis submitted in partial fulfillment
of the requirements for the degree

of

MASTER OF SCIENCE

in

Civil and Environmental Engineering

Approved:

_____	_____
Michael C. Johnson, Ph.D. Major Professor	Steven L. Barfuss, M.S. Committee Member
_____	_____
Marv W. Halling, Ph.D. Committee Member	Laurens H. Smith, Ph.D. Interim Vice President for Research and Dean of the School of Graduate Studies

UTAH STATE UNIVERSITY
Logan, Utah

2019

ABSTRACT

Pressure Loss Coefficients for Large Mitered Elbows with

Diameters Ranging from 36-inches to 144-inches

by

Hayden J. Coombs, Master of Science

Utah State University, 2019

Major Professor: Michael C. Johnson
Department: Civil and Environmental Engineering

When designing a pipeline system, it is important to understand the pressure losses that will occur within the system. One common source of pressure loss is from elbow pipe fittings. There is extensive research available for pressure loss coefficients of elbow pipe fittings, but the research is derived from elbows with relatively smaller pipe diameters. The purpose of this research is to investigate pressure losses associated with larger diameter mitered elbows (36-inches to 144-inches). The dimensions for all mitered elbows considered in this research follow ANSI/AWWA C208-17 recommendations (AWWA 2017).

This research uses computational fluid dynamics to determine the pressure loss coefficients of large mitered elbows, reducing mitered elbows, and expanding mitered elbows. Computational fluid dynamic simulations were compared with physical data to ensure good numerical methods and quality results were produced.

The results suggest a strong correlation that the pressure loss for large mitered elbows, presented in this research, are solely dependent on the pipe Reynolds number. The reducing and expanding mitered elbows showed the pressure loss coefficient is dependent on Reynolds number and the percent of reduction/expansion of the elbow. However, the results' correlation was not as strong as the large mitered elbows, so there may be some additional dependency on pipe diameter size.

Tabulated data, graphical data, and recommended equations are presented to determine pressure loss coefficients for large mitered elbows, reducing mitered elbows, and expanding elbows.

(67 pages)

PUBLIC ABSTRACT

Pressure Loss Coefficients for Large Mitered Elbows with

Diameters Ranging from 36-inches to 144-inches

Hayden J. Coombs

When designing a pipeline system, it is important to understand the pressure losses that will occur within the system. One common source of pressure loss is from elbow pipe fittings. There is extensive research available for pressure loss coefficients of elbow pipe fittings, but the research is derived from elbows with relatively smaller pipe diameters. The purpose of this research is to investigate pressure losses associated with larger diameter mitered elbows (36-inches to 144-inches). The dimensions for all mitered elbows considered in this research follow ANSI/AWWA C208-17 recommendations (AWWA 2017).

Due to the large size of the mitered elbows of interest, physical testing was not feasible for this research. Therefore, this research used numerical methods to determine the pressure loss coefficients of large mitered elbows, reducing mitered elbows, and expanding mitered elbows.

The results suggest a strong correlation that the pressure loss for large mitered elbows, presented in this research, are solely dependent on the pipe Reynolds number. The reducing and expanding mitered elbows showed the pressure loss coefficient is dependent on Reynolds number and the percent of reduction/expansion of the elbow. Tabulated data, graphical data, and recommended equations are presented to determine pressure loss for large mitered elbows, reducing mitered elbows, and expanding elbows.

ACKNOWLEDGMENTS

I would like to thank Dr. Michael Johnson for his guidance and support that was needed to complete this project. I also would like to thank him for the opportunity to work at the Utah Water Research Laboratory. His mentorship and the experiences I had while working at the water lab has led me to the beginning of a fulfilling career that I greatly enjoy.

I would like to thank my other committee members, Steve Barfuss and Dr. Marv Halling, for their suggestions and support given to me. I would also like to thank Dr. Zac Sharp for providing me with essential insights with regard to computational fluid dynamics, and for the many experiences I had while working at the water lab.

Lastly, I am grateful for my wife, McKenzie, for the support, encouragement, and patience she gave me while I finished this research.

Hayden J. Coombs

CONTENTS

Page

LIST OF TABLES

LIST OF FIGURES

Figure Page

Figure Page

LIST OF EQUATIONS

LIST OF VARIABLES

C_1 = Coefficient from Table 4

C_2 = Coefficient from Table 4

D = Diameter of the pipe and/or elbow

D_1 = Inside diameter of the upstream pipe

D_2 = Inside diameter of the downstream pipe

f = Darcy-Weisbach friction factor

f_1 = Darcy-Weisbach friction factor for the upstream pipe

f_2 = Darcy-Weisbach friction factor for the downstream pipe

g = Acceleration due to gravity

ΔH = Net head loss

ΔH_{1-2} = Net head loss between the upstream and downstream pressure taps

K = Pressure loss coefficient

K_{V_1} = Pressure loss coefficient to be used with the upstream velocity

K_{V_2} = Pressure loss coefficient to be used with the downstream velocity

P = Average pressure in the fluid

P_1 = Pressure in the fluid measured at a location upstream from the elbow

P_2 = Pressure in the fluid measured at a location downstream from the elbow

L = Length of pipe

L_1 = Length of pipe between the upstream pressure taps and the elbow

L_2 = Length of pipe between the downstream pressure taps and the elbow

n = Number of 22.5 degree miters in the mitered elbow

R = Radius of the elbow

Re = Reynolds number

V = Average velocity of the fluid

V_1 = Average velocity of the fluid at a location upstream from the elbow

V_2 = Average velocity of the fluid at a location downstream from the elbow

z_1 = Elevation of the centerline of the pipe at a location upstream from the elbow

z_2 = Elevation of the centerline of the pipe at a location downstream from the elbow

Δ = Total deflection of a mitered elbow

γ = Unit weight of the fluid

v = Kinematic viscosity of the fluid

CHAPTER I

INTRODUCTION

Purpose

When designing a pipeline, it is important to understand the sources of pressure loss within the system. Pressure loss can result from pipe friction, valves, flow meters, filters or screens, turbines, pipe fittings, etc.

A common type of pipe fitting that creates pressure loss are elbows. Extensive research is available to help determine the amount of pressure loss from an elbow. However, most of this research has been conducted on relatively small pipe diameter sizes (typically 24-inches or less) because they are more feasible to conduct physical tests in a water research facility.

However, there is little to no research available for pressure losses of larger pipe diameters (up to 144-inches). This is simply due to the impractical requirements to conduct the physical testing needed. Costs would be too high to purchase the required lengths of pipe, the water facility would need a large floor plan, and it is unlikely the facility would have the water capacity to test the elbows over a wide range of velocities. For this reason, it is common practice to use published pressure loss coefficients for elbows over a wide range of pipe diameter sizes.

Elbows for large pipe diameter sizes, however, typically have different dimensions than what the pressure loss coefficients represent. Small pipe diameter sizes use elbows with a smooth rolled bend. It is difficult to manufacture smooth elbows for

larger pipe diameter sizes, so it is common to manufacture a mitered elbow. The two types of elbows are shown in Figure 1. A mitered elbow is made by cutting the pipe at a

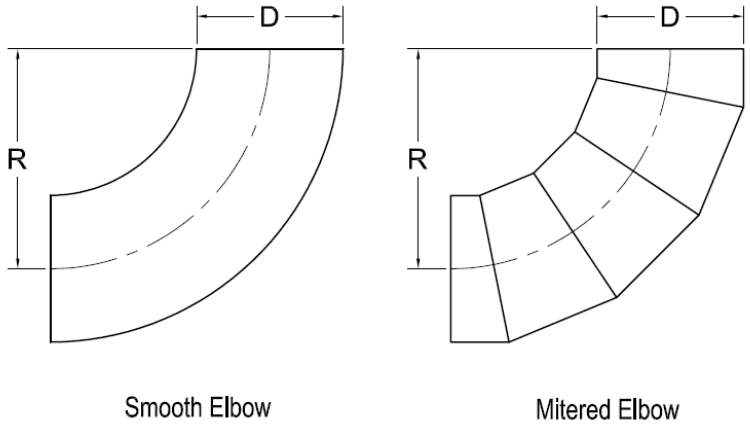

Figure 1. Types of elbows

desired angle several times, rotating the cut pipe segments along its axis 180 degrees, and welding the joints together. A benefit to using mitered elbows is the flexibility to manufacture them to meet field conditions. An important dimension when considering elbows is the ratio of the elbow's radius of curvature with the diameter of the elbow, R/D. Elbows with a R/D ratio of 1.5 are commonly referred to as long radius elbows.

Research has been conducted for smaller mitered elbows to investigate how the pressure loss might differ from a regular smooth elbow, but their dimensions are inconsistent due to the flexibility of how they are manufactured.

Objectives

The objective of this research was to investigate the pressure losses associated with large diameter mitered elbows. Furthermore, the research investigates pressure loss dependency from the pipe's Reynolds number, which is defined in Equation 1.

$$Re = \frac{VD}{v}$$

Equation 1. Reynolds number

where Re is the Reynolds number, V is the average velocity of the fluid, and v is the kinematic viscosity of the fluid.

In order to perform this research, computational fluid dynamics (CFD) methods were used. CFD is changing the engineering industry as technology advances and numerical methods improve. CFD simulations are also more feasible for this research than physical testing, for reasons already mentioned. CFD methods, however, are not perfect and can easily be misinterpreted. For this reason, CFD simulations will be compared with pressure loss coefficients published from physical testing. Once the comparisons are acceptable, similar CFD methods were reproduced for researching the large mitered elbows.

Scope of Work

An important aspect for this research was the need to establish a commonality and scope for the dimensions of the mitered elbows. For this reason, the mitered elbows tested in this research follow the recommendations of ANSI/AWWA C208-17; namely, the elbow has R/D a ratio of 2.5, and each miter shall not have a deflection greater than 22.5 degrees (AWWA, 2017).

The mitered elbows, found in Figure 2, have pipe diameters of 36-inch, 48-inch, 72-inch, 96-inch, and 144-inch. The reducing and expanding mitered elbows, found in Figure 3, have pipe diameters of 60-inch and 120-inch with a percent reduction in pipe diameter of 10%, 30%, and 50%. Therefore, the reducing and expanding miter elbows

included in this research are 60 x 54-inch, 60 x 42-inch, 60 x 30-inch, 120 x 108-inch, 120 x 84-inch, and 120 x 60-inch. All mitered elbows considered in this research were assumed to have schedule 40 thickness.

The CFD simulations used in this research considered velocities ranging from 4 to 20 feet per second (for the reducing and expanding mitered elbows, this range of velocity applies to the larger pipe diameter).

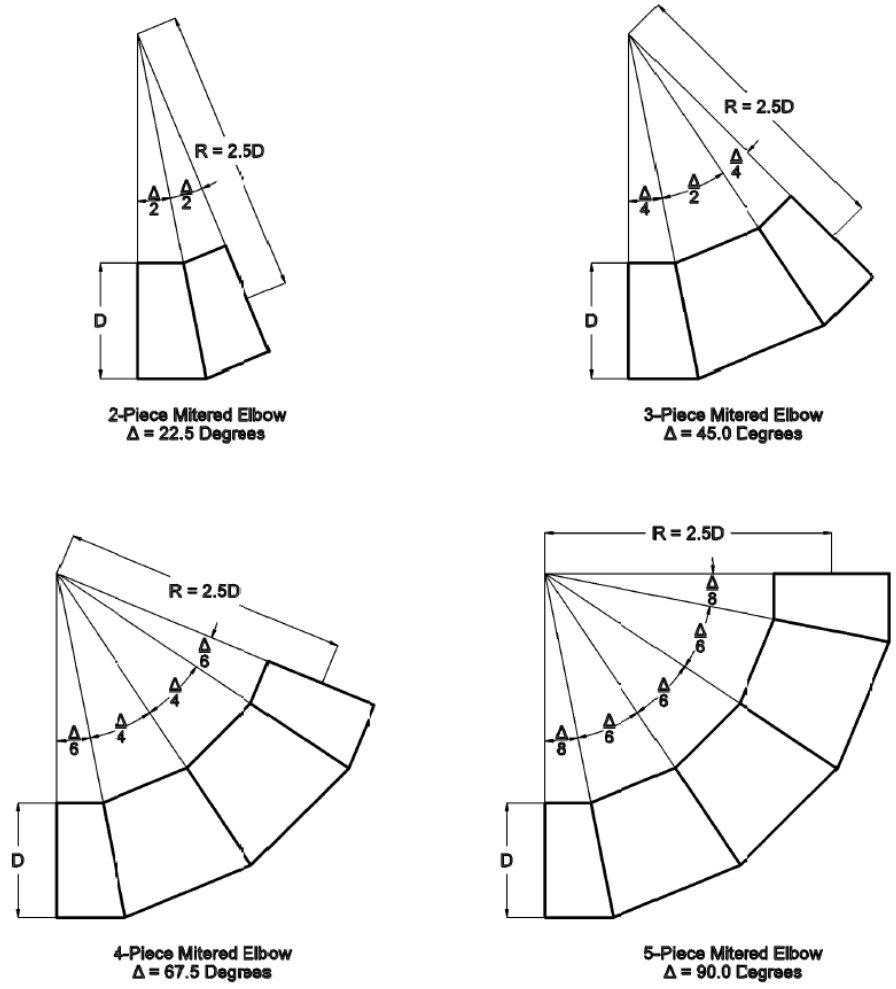

Figure 2. General dimensions of large mitered elbows

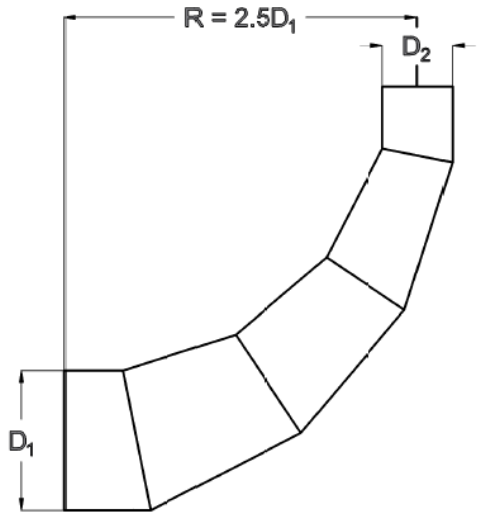

Figure 3. General dimensions for reducing and expanding mitered elbow

CHAPTER II

LITERATURE REVIEW

Pressure losses from valves, meters, pipe fittings, etc., are commonly denoted by a coefficient, K, which is calculated from the Darcy-Weisbach equation (Equation 1).

$$\Delta H = K\frac{V^2}{2g}$$

Equation 2. Darcy-Weisbach local head loss

where ΔH is the net head loss (pipe friction between pressure measurement points is not included) in the fluid, K is the pressure loss coefficient, V is the average velocity of the fluid, and g is the acceleration due to gravity.

This section will describe the sources of pressure loss from elbows and previous research that has been performed to determine *K* for elbows for smooth and mitered elbows.

Sources of Pressure Loss from Elbows

I.E. Idelchick's research identifies the sources of pressure loss resulting from elbow fittings. Idelchick explains that the separation of flow that occurs in an elbow causes centrifugal forces that account for several sources of pressure loss: a separation of flow on the inner curve of the elbow and later on the outer wall, a presence of local high and low pressures, eddy zones, streamlines that form in a helix, and more (Idelchick 2008).

D.S. Miller includes several diagrams of cross-sectional velocity profiles and how they change with respect to distance downstream from the elbow. The elbow causes a concentration of high velocity on the inner wall of the bend. Immediately after the bend, there is a local concentration of low pressures and eddies. Miller explains that this imbalance of pressures and velocities cause the flow to turn and converge towards the low pressure zones, which leads to swirls that can extend far downstream from the elbow (Miller 2011).

Crane Company also comments on the unique headloss from the swirls that are associated with elbows. Crane Co. refers this swirl as secondary flow and defines it as a "rotation motion, at right angles to the pipe axis, which is superimposed upon the main motion in the direction of the axis" (Crane 2010).

Pressure loss from turbulence in swirls will continue far downstream from an elbow. ISO 5419 states the axial profile should be within 5% of a fully developed flow profile after 100 diameters of straight pipe after close-coupled elbows (ISO 1991). For other applications, such as a valve, it is common to measure pressure only six diameters downstream (AWWA 2017). This research will follow the AWWA standards for measuring pressure six diameters downstream, but it is important to note that additional pressure loss is occurring beyond this point.

Idelchick lists several aspects that can contribute to *K* for an elbow: Reynolds number, relative roughness of the pipe walls, inlet flow conditions, and the dimensions of the elbow. Two important dimensions that will affect the elbow's *K* is the radius of the bend and the change of cross-sectional area through the elbow, if any (Idelchick 2008).

Previous Research on Pressure Loss Coefficients for Smooth and Mitered Elbows

Idelchick performed tests to determine *K* for mitered elbows with pipe diameter sizes ranging from 50-millimeters to 350-millimeters (approximately 2-inches to 14-inches) and R/D ratios ranging from 0.5 to 15. A *K* of 0.12 was reported for a mitered elbow with a 90 degree bend, four 22.5 degree miters, and a R/D ratio of 2.5 (Idelchick 2008).

D.S. Miller's method for determining *K* for a mitered elbow consisted of defining an initial *K* for a specific type of elbow at a Reynolds number of 10^6. The *K* would then be adjusted by three coefficients that represented differences in Reynolds number, relative roughness for pipe friction, and outlet pipe conditions. Miller's R/D ratios for mitered elbows ranged from 0.5 to 6. Miller's research reported a *K* of 0.22 for a mitered elbow with a 90 degree bend, four 22.5 degree miters, and a R/D ratio of 2.5 (Miller 2011).

Crane Co. only references data for mitered elbows with one miter ranging from 0 degrees to 90 degrees in 15 degree increments. Their method for solving for *K* is multiplying a friction factor to a table of coefficients that are dependent on the deflection of the miter. No information is given for the R/D ratios that these *K*s should be applied to (Crane 2010).

W. Rahmeyer did not conduct research on mitered elbows, but his research on smooth elbows provided insightful direction for this research. Rahmeyer's research suggested that *K* is dependent on pipe velocity. He concluded that as velocity increases, *K* decreases. His research also suggested that *K* is dependent on the pipe diameter

(Rahmeyer 1999). It is common engineering practice apply the same *K* for a pipe fitting over a wide range of velocities, but Rahmeyer's research suggests there is error in this method. The sizes of smooth elbows in Rahmeyer's study were 2-inch, 4-inch, and a 4 x 3-inch reducing elbow. They all had R/D ratios of 1.5. The range of velocities tested for the smooth elbows was 1 feet per second to 12 feet per second (Rahmeyer 1999).

P. Koch realized the need to expand *K* over a range instead of having a single value to be used for any pipe size diameter or any Reynolds number. Koch's research mainly consists of compiling pressure loss coefficient data that has been determined by physical experiments. A lot of data is presented in Koch's findings, and it verifies that *K* is dependent on pipe diameter and Reynolds number. However, his graphs only consider one of the two concepts (Koch 2006). For example, a graph might display how *K* varies with pipe diameter, but the graph is representative of only one Reynolds number.

P. Dent performed similar tests as Rahmeyer, and he came to the same conclusion that *K* is dependent on velocity and pipe diameter. Dent's research included larger sized smooth elbows of 12-inch, 16-inch, 20-inch, and 24-inch pipe diameters; all had a R/D ratio of 1.5. Dent also increased the velocity range to 20 feet per second (Dent 2000). Dent's research was valuable for this study because it was some of the largest sized elbows and more recent *K*s that have been published. His data will be used to compare with CFD simulations, which will be further described later in this thesis.

C. Ding et al. also performed similar research as Rahmeyer, but with smooth elbows with pipe diameters of 6-inch, 8-inch, and 10-inch diameters; all had a R/D ratio of 1.5. Ding also concluded that *K*s for elbows are dependent on velocity and pipe

diameter (Ding et al. 2005). A particular elbow of interest was Ding's physical testing of an 8 x 10-inch expanding elbow. This elbow will be used for CFD simulations conducted in this research.

There is an extensive amount of research that investigates pressure loss correlations in pipe fittings, particularly for HVAC systems. S. F. Moujaes and S. Deshmukh used STAR-CD software and CFD methods to investigate pressure drops in pipe elbows (Moujaes and Deshmukh 2006). Their process for incorporating CFD software provided insight for the numerical procedures that will be presented in this research.

CHAPTER III

PRESSURE LOSS COEFFICIENTS

In order to determine *K* in Equation 2 for a valve, meter, pipe fitting, etc., it is necessary to know the net head loss that the item of interest causes. The net head loss in the fluid can be found by using Bernoulli's energy equation (Equation 3).

$$\frac{V_1^2}{2g} + \frac{P_1}{\gamma} + z_1 = \frac{V_2^2}{2g} + \frac{P_2}{\gamma} + z_2 + \frac{f_1 L_1}{D_1}\frac{V_1^2}{2g} + \frac{f_2 L_2}{D_2}\frac{V_2^2}{2g} + \Delta H_{1-2}$$

Equation 3. Energy equation

where P is the average pressure in the fluid, z is the elevation of the centerline of the pipe, γ is the unit weight of the fluid, f is the Darcy-Weisbach friction factor, L is the distance from the pressure taps to the item being tested (for this research, the item is a mitered elbow), and D is the inside diameter of the pipe. The subscripts *1* and *2* denotes location of pressure taps upstream and downstream of the mitered elbow, respectively.

Solving for the net head loss in Equation 3 produces Equation 4.

$$\Delta H_{1-2} = \frac{V_1^2 - V_2^2}{2g} + \frac{P_1 - P_2}{\gamma} + z_1 - z_2 - \frac{f_1 L_1}{D_1}\frac{V_1^2}{2g} - \frac{f_2 L_2}{D_2}\frac{V_2^2}{2g}$$

Equation 4. Net head loss

Equation 5 is made when considering both Equations 2 and 4. Note that *K* in Equation 5 is related to a specified velocity in the pipe. This is an important concept when considering a pipe fitting that reduces or expands in pipe diameter. For example, if *K* is defined as K_1, then the upstream velocity should be used to calculate the correct net head loss.

$$K_{V_i} = \frac{2g\Delta H_{1-2}}{V_i^2}$$

Equation 5. Pressure loss coefficient

Although *K* can be defined by either the upstream or downstream velocity, it is fairly common to define *K* by the faster velocity. This is because the smaller pipe diameter is likely to control the limitations of the system. This research, however, will use the slower pipe velocity in order to investigate correlations of *K* with a common pipe diameter (i.e. reducing and expanding elbows with 120 x 108-inch, 120 x 84-inch, and 120 x 60-inch pipe diameters).

All physical testing and numerical methods use Equations 4 and 5 to determine the pressure loss coefficients presented in this research.

CHAPTER IV

PHYSICAL TEST SETUP AND PROCEDURES

The purpose of physical testing was to acquire data for the CFD simulation comparison. This section will describe the test set up and procedures for two elbows that were tested at the Utah Water Research Laboratory (UWRL) in Logan, Utah. Published data for other elbows were also used for CFD comparisons.

Physical Testing at the UWRL

In order to compare CFD simulations of flow in mitered elbows, a 2-inch diameter 90 degree mitered elbow was manufactured for physical testing (see Figure 4). The 2-inch mitered elbow was made of schedule 40 steel pipe, consisted of four pieces with three 30 degree miters, and featured a R/D ratio of 2.5. The elbow was welded to class 150 flanges. Welding debris, metal burrs, and edges were removed to ensure smooth transitions between mitered pieces.

Due to the difficulty of manufacturing a small reducing miter elbow, a smooth 4 x 3-inch smooth elbow was tested at the UWRL (see Figure 5). The reducing elbow was featured schedule 40 steel, class 150 flanges, and a R/D ratio of 1.5.

The elbows were carefully installed to ensure they were level and that there was a smooth transition between the pipe and the elbow. According to AWWA standards, pressure taps were located two diameters upstream from the elbow and six diameters downstream from the elbow (AWWA 2017). Pressure measurements were made using

precision pressure transmitters. To ensure a nearly uniform and fully-developed approach velocity, the upstream pipe had a minimum length of 20 diameters.

Figure 4. Installation of 2-inch mitered elbow for physical testing

Each test set up featured a magnetic flow meter that was calibrated against a NIST traceable weight tank capable of ±0.25% accuracy. For the 2-inch miter elbow, flows were measured with a 2-inch magnetic flow meter and a NIST traceable weight. The flows for the 4 x 3-inch reducing smooth elbow were measured with a 6-inch magnetic flow meter. The elbows were tested for velocities ranging from 2 feet per

second to 20 feet per second. Control valves were located at least 40 pipe diameters downstream to set the desired flow in the system.

Equations 4 and 5 were used to determine *K* for the elbows. Velocities were determined by dividing the flow by the area of the pipe. Pipe friction was accounted for by using common friction factors for steel pipe.

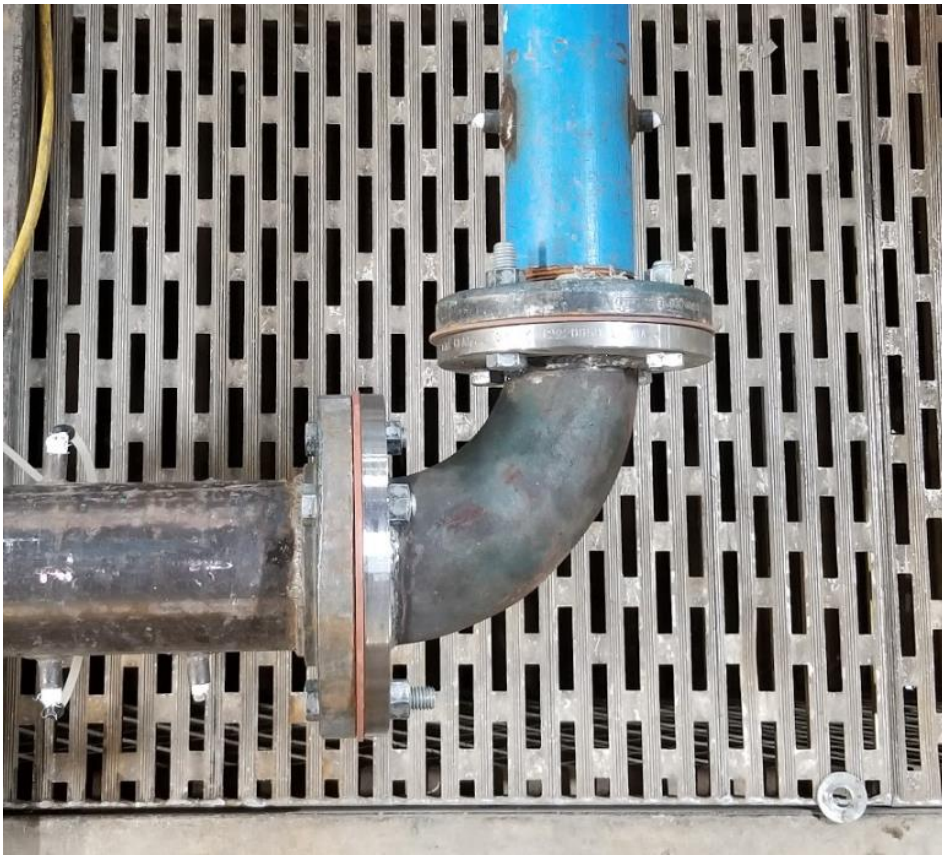

Figure 5. Installation of 4 x 3-inch reducing smooth elbow for physical testing

Published Data

Although the elbows tested at the UWRL were helpful for CFD comparisons, larger elbows were needed to ensure accurate modeling in case of scale effects. The pressure loss coefficients from Dent's and Ding's research were used. The 16-inch and 20-inch smooth elbows' *K*s were used from Dent's research, and the 8 x 10-inch expanding elbow's *K*s from Ding's research. The pressure tap locations for Dent's research are the same as performed at the UWRL; two diameters upstream from the elbow and six diameters downstream. Ding's research, however, used pressure taps located 1.5 diameters upstream from the elbow and 20 diameters downstream. The CFD simulations took pressure and velocity measurements from the same locations that Dent and Ding used for their respective research.

CHAPTER V

NUMERICAL MODELING: CFD METHODS

Test Setup and Procedures

The numerical procedure for determining *K* for the elbows in the CFD simulations are similar to the physical tests. A fully-developed velocity profile was imported to the inlet of the CFD model. A Darcy-Weisbach friction factor was also determined from a section of pipe with a fully-developed velocity profile. Average pressure and velocity values were extracted from cross-sectional planes located two diameters upstream from the elbow and six diameters downstream (except when modeling Ding's research in which this case it was 1.5 diameters upstream and 20 diameters downstream), which also satisfies AWWA's recommendations (AWWA 2017). Due to ISO's findings about swirls occurring far downstream from elbows, the pressure recovery was monitored downstream from the elbow to ensure near-full recovery. If there was an instance where pressure recovery was not achieved, the downstream measuring point was moved appropriately. *K*s were determined by Equations 4 and 5.

All simulations were monitored until acceptable convergence was achieved (residuals were less than 0.0001).

Determining the CFD Methods

All CFD simulations were performed at the UWRL in Logan, Utah using Star CCM+ software (CD-adapco 2018). This section describes aspects of numerical modeling that were considered when determining the best CFD methods for this research.

The methods were determined by comparing the accuracy of the CFD simulations with the physical tests performed at the UWRL and other published data.

Star CCM+ offers a variety of CFD models to satisfy the Reynolds-Averaged Navier-Stokes equations (CD-adapco 2018). Star CCM+'s Realizable κ-ε (Rκ-ε) and Standard κ-ε (Sκ-ε) are common models used in a wide variety of applications. Other models were also initially considered for the purpose this research, but it was quickly determined that the Rκ-ε and Sκ-ε modes produced better results.

Star-CCM+ gives the user the option to use hydraulically smooth pipes or to incorporate a roughness height when modeling the pipe friction in the simulation. Both options were tested in the CFD models when comparing with the physical test results.

Another important concept when considering numerical modeling is steady-state flow versus unsteady-state flow. Steady-state models perform adequate results for most pipeline applications. However, because of the flow separation and swirls that occur from an elbow, unsteady-state simulations were considered. After several CFD simulations were made, the unsteady-state models produced almost identical results as the steady-state models; therefore, a steady-state model was used for the CFD simulations performed in this research.

Mesh Quality Procedures

For most numerical modeling techniques, it is required to have a mesh for the model to satisfy the governing equations (in this case, the Reynolds-Average Navier-Stokes equation). While numerical modeling is an effective method to provide insight to various fluid mechanic and hydraulic applications, it can be easy to produce inaccurate

data due to incorrect meshing techniques. For this reason, this research followed the Grid Convergence Index (GCI) method (Celik et al. 2008). The GCI method ensures that the grid cell size is small enough to produce accurate results. This process requires that a simulations grid cell size be increased and decreased by a factor of at least 1.3. If the change in the solution of the simulation was unacceptable, then the original cell size should be reduced and checked for mesh quality again.

Due to the large amount of CFD simulations that was conducted in this research and the similarity of the geometry of the simulations, the GCI method was not performed for each simulation. Instead, the simulations with the most extreme circumstances were checked for mesh quality. For example, CFD simulations with the low and high end velocities where checked for the smaller and larger pipe diameter simulations. Once meshing techniques were acceptable by the GCI method, they were repeated for all other simulations.

CHAPTER VI

RESULTS AND DISCUSSION

CFD Results in Comparison with Physical Data

The first set of physical data that was compared with CFD simulations was Dent's 16-inch and 20-inch diameter smooth elbows. Several models offered by Star-CCM+ were tested in this phase, which the Rκ-ε results proved to be the most accurate. The Rκ-ε model was used to compare simulations with hydraulically smooth pipe walls and rough pipe walls. Figures 6 and 7 displays the results, which suggest that the hydraulically smooth pipe simulations would produce more accurate results. The maximum absolute errors for the 16-inch and 20-inch diameter smooth elbows for the smooth pipe wall simulations were 2.2% and 8.0%, respectively. The remaining CFD simulations were tested with hydraulically smooth pipe walls.

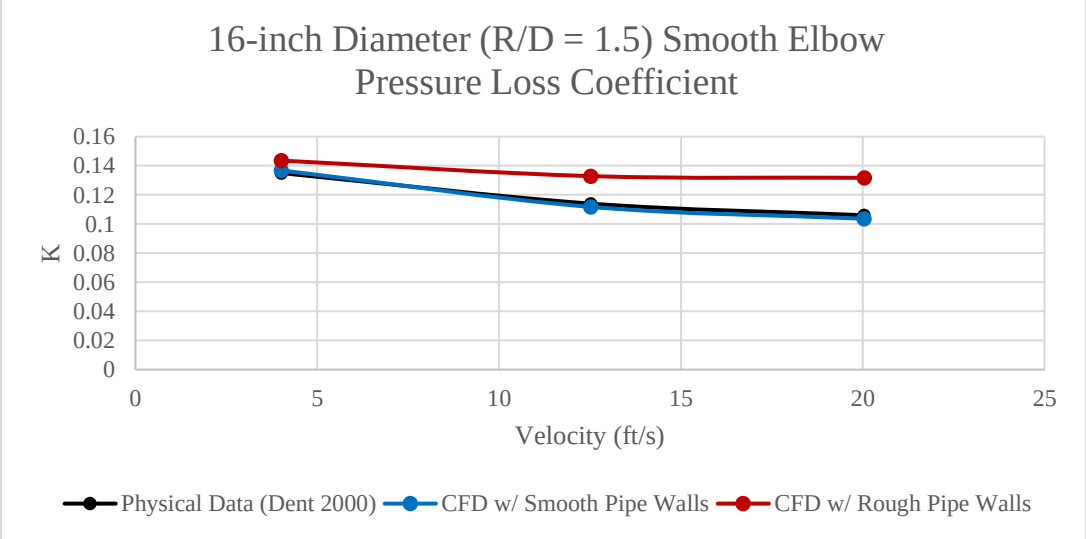

Figure 6. CFD Rκ-ε comparison of physical data for a 16-inch diameter smooth elbow

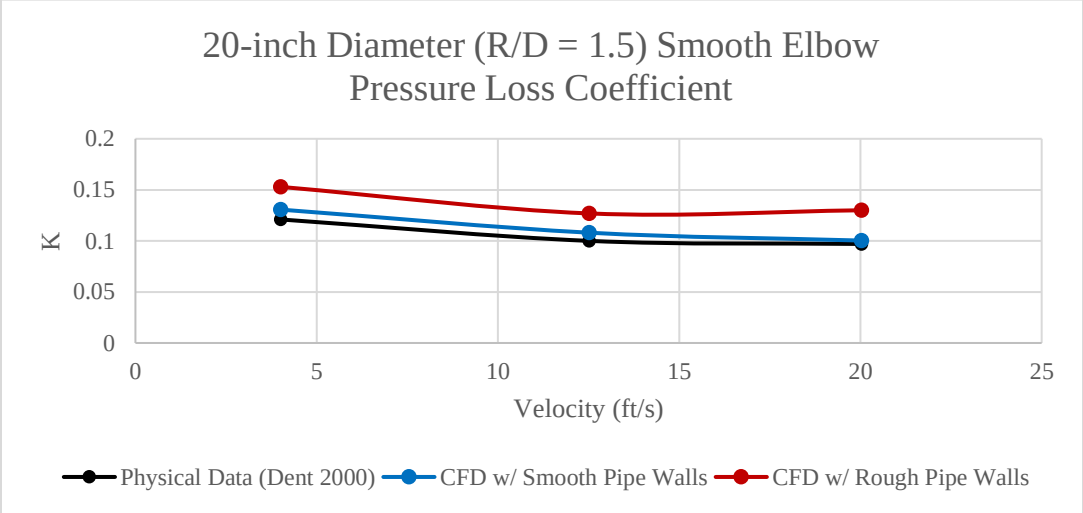

Figure 7. CFD Rκ-ε comparison of physical data for a 20-inch diameter smooth elbow

The 2-inch mitered elbow was then modeled with the same conditions: smooth pipe walls and a Rκ-ε solver. The CFD results produced a maximum absolute error of 10.3%. The results can be seen in Figure 8.

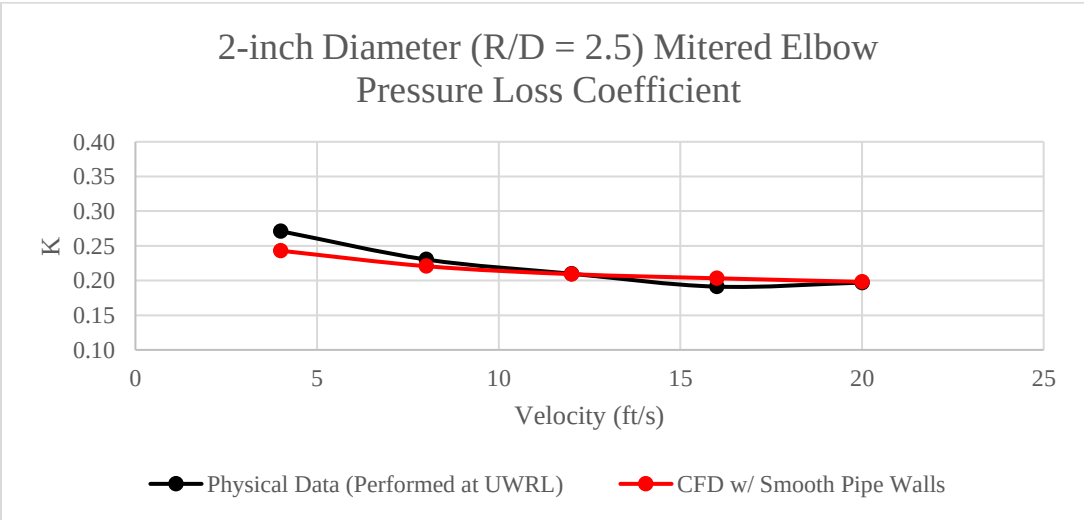

Figure 8. CFD Rκ-ε comparison of physical data for a 2-inch diameter mitered elbow

The last set of physical data to be tested against CFD simulations was the 4 x 3-inch smooth reducing elbow and the 8 x 10-inch expanding elbow. Due to the more complex streamlines produced by the reducing and expanding elbows, the CFD simulations considered two models: Rκ-ε and Sκ-ε. Figure 9 and 10 displays the CFD results of the two elbows. The Rκ-ε produced more inconsistent results of the two elbows. For the reducing elbow, the Rκ-ε under accounted for pressure loss with a deviating error of -16.5%. The Rκ-ε overestimated the results for the expanding elbow results with a deviating error of 34.0%. The Sκ-ε model, however, produced more consistent data for both elbows. The reducing and expanding elbow had deviating errors of 13.6% and 10.6% produced from the Sκ-ε model, respectively. For this reason, it was decided to use the Sκ-ε model for the large reducing and expanding mitered elbows. The model was more consistent and accurate, plus it suggested to be more conservative.

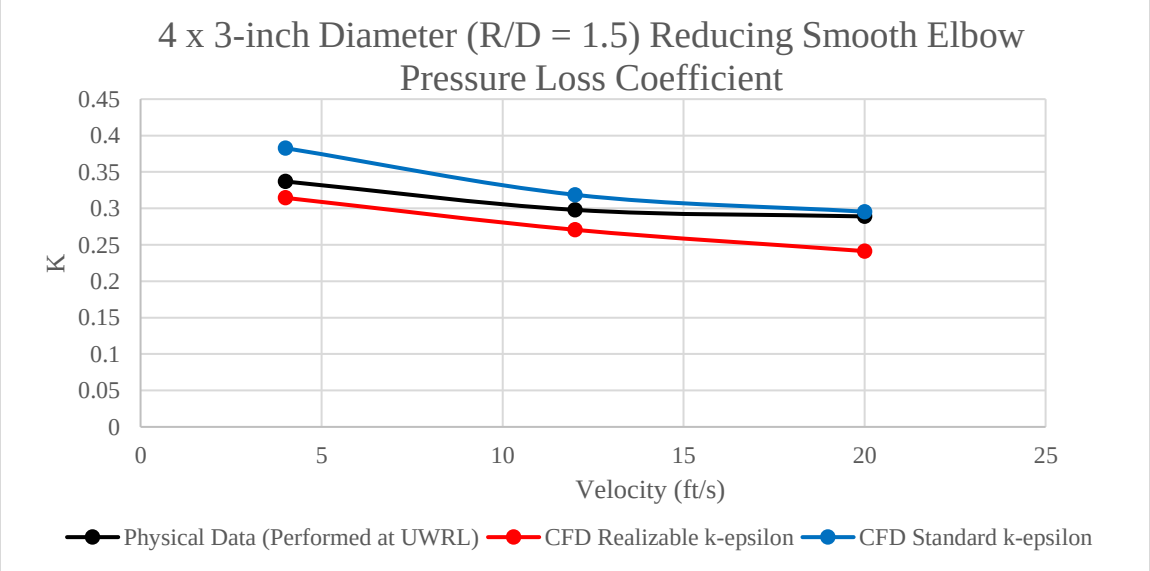

Figure 9. CFD Rκ-ε and Sκ-ε comparisons of physical data for a 4 x 3-inch diameter reducing smooth elbow

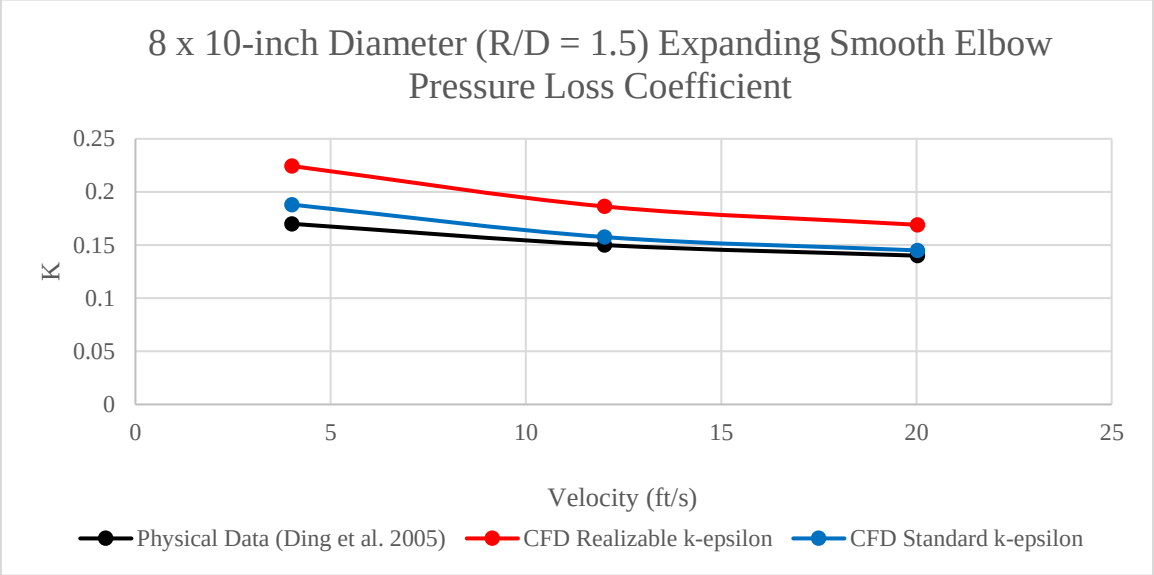

Figure 10. CFD Rκ-ε and Sκ-ε comparisons of physical data for an 8 x 10-inch diameter expanding smooth elbow

In summary, it was decided to model all CFD simulations with hydraulically smooth pipe walls, simulate the large mitered elbows with Rκ-ε models, and simulate the reducing and expanding mitered elbows with Sκ-ε models. The CFD and physical testing tabulated results can be found in Table 1.

Table 1. Comparison of pressure loss coefficients from CFD simulations and physical testing

Description	Source of Physical Data	Velocity (ft/s)	Physical K	CFD*		CFD†	
				K	Error (%)	K	Error (%)
16-inch diameter smooth elbow	Dent 2000	4	0.135	0.137	1.4%	0.144	6.3%
		12.5	0.114	0.112	-2.0%	0.133	16.6%
		20	0.106	0.104	-2.2%	0.132	24.3%
				CFD*		CFD†	
20-inch diameter smooth elbow	Dent 2000	4	0.121	0.131	8.0%	0.153	26.4%
		12.5	0.100	0.108	8.0%	0.127	26.9%
		20	0.097	0.100	3.4%	0.130	34.0%
				CFD*			
2-inch diameter mitered elbow	Performed at UWRL	4	0.271	0.243	-10.3%	-	-
		8	0.230	0.221	-3.9%	-	-
		12	0.210	0.209	-0.5%	-	-
		16	0.191	0.203	6.3%	-	-
		20	0.197	0.198	0.5%	-	-
				CFD*		CFD‡	
4 x 3-inch diameter reducing smooth elbow	Performed at UWRL	4	0.337	0.315	-6.7%	0.383	13.6%
		12	0.298	0.271	-9.2%	0.319	6.9%
		20	0.289	0.241	-16.5%	0.295	2.2%
				CFD*		CFD‡	
8 x 10-inch diameter expanding smooth elbow	Ding et al. 2005	4	0.170	0.224	32.0%	0.188	10.6%
		12	0.150	0.186	24.2%	0.158	5.0%
		20	0.140	0.169	20.8%	0.145	3.6%

*CFD methods include a steady-state Realizable κ-ε model with hydraulically smooth pipe walls.
†CFD methods include a steady-state Realizable κ-ε model with relative roughness of e = 0.0002 ft.
‡CFD methods include a steady-state Standard κ-ε model with hydraulically smooth pipe walls.

CFD Results for the Large Mitered Elbows

Due to Rahmeyer, Dent, and Ding focusing their research on *K* dependency from pipe velocities, the plots thus far have been focused on velocity. However, to incorporate dependency on both pipe velocity and diameter, the CFD results for the large mitered elbows have been plotted with relationship to Reynolds number. The graphical data for the CFD simulations of large mitered elbows are given in Figure 11; the tabulated data can be found in Table 2.

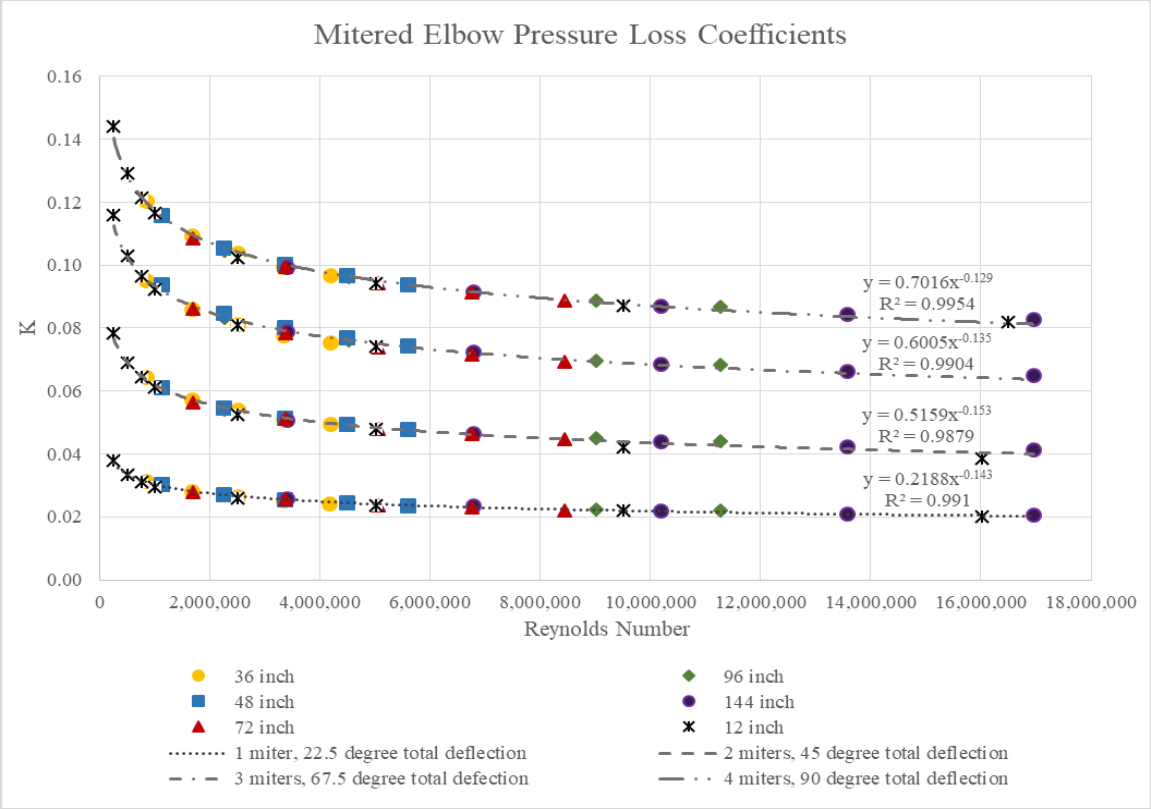

Figure 11. Pressure loss coefficients for large mitered elbows (R/D = 2.5) produced by CFD simulations

The correlation of *K* and Reynolds number for large mitered elbows seemed strong enough to suggest that *K* for mitered elbows (and possibly smooth elbows) are solely dependent on Reynolds number. To support this claim, similar CFD simulations were made for a 12-inch mitered elbow (which followed the same AWWA recommendations for mitered elbow dimensions). The 12-inch mitered elbow results are included in the graphical data found in the Figure 11, and they confirm the suggestion that *K* is solely dependent on Reynolds number.

It was also found that the pressure downstream from the elbow was fully recovered before the pressure taps located six diameters downstream, but there was still a

presence of swirls in the flow. An example of the velocity profiles, pressure recovery, and streamlines of a 72-inch mitered elbow can be found in Appendix A.

Table 2. Pressure loss coefficients for large mitered elbows (R/D = 2.5) produced by CFD simulations

Total Deflection	Velocity, V_1 (fps)	Pressure Loss Coefficient, K_{V1}				
		D = 36 inch	D = 48 inch	D = 72 inch	D = 96 inch	D = 144 inch
22.5° (1 miter)	4	0.032	0.030	0.028	0.027	0.026
	8	0.028	0.027	0.026	0.025	0.024
	12	0.027	0.026	0.024	0.023	0.022
	16	0.025	0.025	0.023	0.022	0.021
	20	0.024	0.024	0.022	0.022	0.021
45° (2 miters)	4	0.064	0.061	0.056	0.054	0.051
	8	0.057	0.055	0.051	0.049	0.047
	12	0.054	0.052	0.048	0.046	0.044
	16	0.051	0.050	0.046	0.045	0.042
	20	0.050	0.048	0.045	0.044	0.042
67.5° (3 miters)	4	0.095	0.094	0.086	0.083	0.079
	8	0.086	0.085	0.078	0.076	0.073
	12	0.081	0.080	0.074	0.072	0.069
	16	0.078	0.077	0.071	0.070	0.066
	20	0.075	0.075	0.069	0.068	0.065
90° (4 miters)	4	0.120	0.116	0.108	0.105	0.099
	8	0.110	0.106	0.099	0.096	0.092
	12	0.104	0.100	0.094	0.092	0.087
	16	0.100	0.097	0.091	0.089	0.085
	20	0.097	0.094	0.089	0.087	0.083

CFD Results for the Large Reducing and Expanding Mitered Elbows

The graphical *K* data for the CFD results of the large reducing and expanding elbows can be found in Figures 12 and 13; the tabulated data can be found in the Table 3.

While the results suggest a strong correlation between *K* and Reynolds number for reducing and expanding mitered elbows, there may be more dependency on diameter.

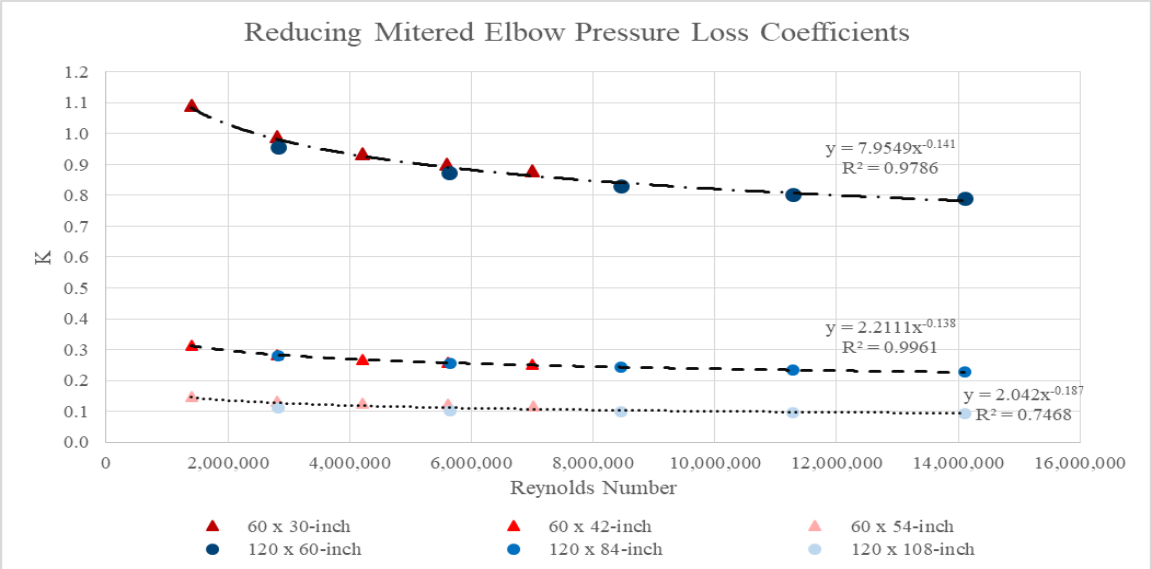

Figure 12. Pressure loss coefficients for reducing mitered elbows (R/D = 2.5) produced by CFD simulations

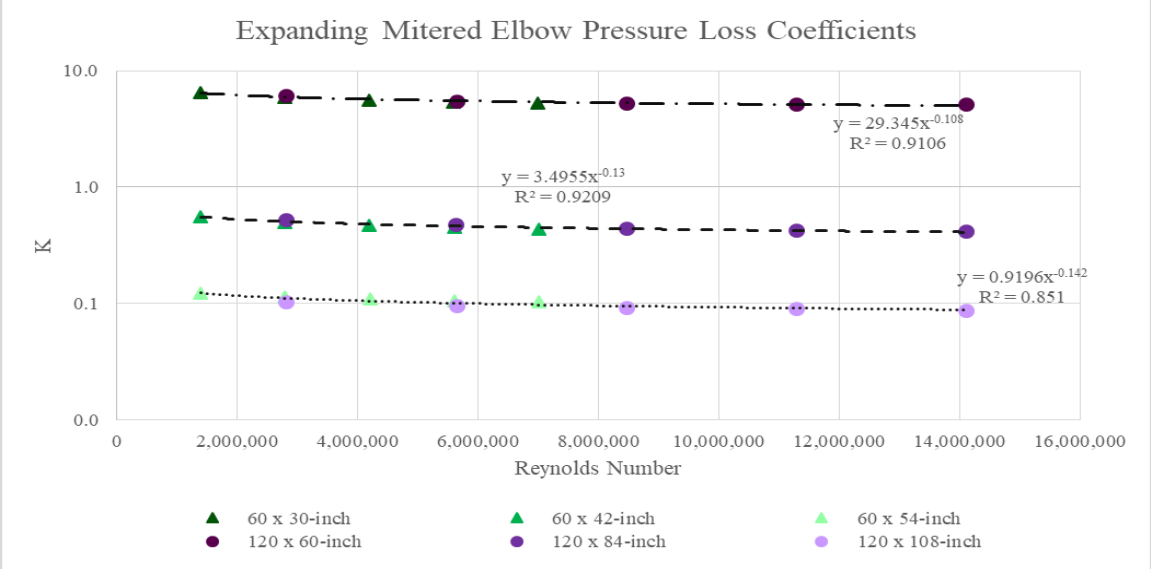

Figure 13. Pressure loss coefficients for expanding mitered elbows (R/D = 2.5) produced by CFD simulations

Table 3. Pressure loss coefficients for large reducing and expanding mitered elbows (R/D = 2.5) produced by CFD simulations

% Reduction (D_2/D_1)	Velocity, V_i (fps)	Reducing Mitered Elbow, K_{V1}		Expanding Mitered Elbow, K_{V2}	
		60 inch x 54 inch	120 inch x 108 inch	54 inch x 60 inch	108 inch x 120 inch
10%	4	0.146	0.112	0.124	0.104
	8	0.132	0.103	0.113	0.096
	12	0.126	0.098	0.109	0.092
	16	0.123	0.095	0.106	0.090
	20	0.119	0.093	0.104	0.088
		60 inch x 42 inch	120 inch x 84 inch	42 inch x 60 inch	84 inch x 120 inch
30%	4	0.314	0.280	0.558	0.526
	8	0.284	0.255	0.500	0.474
	12	0.268	0.242	0.468	0.446
	16	0.259	0.234	0.448	0.428
	20	0.251	0.227	0.432	0.416
		60 inch x 30 inch	120 inch x 60 inch	30 inch x 60 inch*	60 inch x 120 inch*
50%	4	6.532	6.073	0.086	0.083
	8	5.953	5.505	0.078	0.076
	12	5.549	5.309	0.074	0.072
	16	5.326	5.200	0.071	0.070
	20	5.221	5.158	0.069	0.068

*Downstream pressure taps were moved to 15 diameters downstream from mitered elbow for full pressure recovery.

The pressure recovered before the pressure taps located six diameters for all reducing and expanding mitered elbows, except for the expanding elbows with 50% reduction (the 30 x 60-inch expanding mitered elbow and the 60 x 120-inch expanding mitered elbow). It was observed that the pressure recovered approximately 12 pipe diameters downstream, but the pressure taps were moved to 15 diameters downstream to be conservative. The reducing and expanding mitered elbows also displayed swirls

extending far downstream from the elbows. An example of velocity profiles for reducing and expanding mitered elbows can be found in Appendix B and C, respectively.

Mesh Quality

As previously mentioned, the GCI method was not applied to all simulations because of the similarity of geometry and meshing procedures. Table 4 displays the GCI results for gross head loss in inches for the 48-inch 67.5 degree total deflection miter elbow and the 144-inch 90 degree total deflection miter elbow with a pipe velocity of 4 feet per second and 20 feet per second. The GCI was held beneath 2.6% for all simulations, and most of them were below 1%.

Table 4. GCI results of four CFD simulations

Mesh Quality - Grid Convergence Index Method				
Parameter	48" Diameter Mitered Elbow (Δ = 67.5 degrees)		144" Diameter Mitered Elbow (Δ = 90 degrees)	
	V = 4 fps	V = 20 fps	V = 4 fps	V = 20 fps
r_{21}	1.455	1.455	1.343	1.343
r_{32}	1.438	1.438	1.319	1.319
f_1	0.532	10.380	0.500	10.179
f_2	0.526	10.339	0.492	10.057
f_3	0.517	10.258	0.490	10.040
p	1.144	1.924	4.013	6.372
$q(p)$	0.039	0.045	0.105	0.135
s	1	1	1	1
f^{21}_{ext}	0.543	10.419	0.503	10.201
f^{32}_{ext}	0.543	10.419	0.493	10.060
e^{21}_{a}	1.09%	0.40%	1.61%	1.20%
e^{21}_{ext}	2.00%	0.37%	0.70%	0.22%
GCI^{21}_{fine}	2.55%	0.47%	0.89%	0.27%

Application of the Results

Equation 6 should be used to determine the head loss caused by a mitered elbow. Note that the *K* should be used with the associated velocity.

$$\Delta H_{1-2} = K_{V_i} \frac{V_i^2}{2g}$$

Equation 6. Mitered elbow head loss

There are three methods to determine *K* for a mitered elbow:

1. *K* can be determined from Figures 11-13 or from Tables 2 and 3.
2. Since the data suggests that *K* is independent of pipe diameter and only dependent on Reynolds number, K_{V_i} can be determined by the relationship in Equation 6 with the appropriate C_1 and C_2 coefficients found in Table 5.

$$K_{V_i} = C_1 Re^{C_2}$$

Equation 7. *K* equation for mitered elbows

3. It can be observed from Table 2 that *K* is additive with respect to the number of 22.5 degree miters in the elbow. Therefore, Equation 7 can be simplified to Equation 8 (n is the number of 22.5 degree miters in the elbow). The maximum, minimum, and average errors when comparing Equation 8 with Tables 1 and 2 are 4%, -6.5%, ±1.6%, respectively. It is important to note that this method is **not** applicable to determine *K* for reducing and expanding mitered elbows.

$$K_{V_i} = n * (0.2188 Re^{-0.143})$$

Equation 8. Modified *K* equation for mitered elbows

Table 5. Coefficients for Equation 7 and their R^2 values

Mitered Elbow Description	C_1	C_2	R^2
Mitered elbow, total deflection of 22.5°	0.2188	-0.143	0.9910
Mitered elbow, total deflection of 45°	0.5159	-0.153	0.9879
Mitered elbow, total deflection of 67.5°	0.6005	-0.135	0.9904
Mitered elbow, total deflection of 90°	0.7016	-0.129	0.9954
Reducing mitered elbow, 10% reduction	2.0420	-0.187	0.7468
Reducing mitered elbow, 30% reduction	2.2111	-0.138	0.9961
Reducing mitered elbow, 50% reduction	7.9549	-0.141	0.9786
Expanding mitered elbow, 10% reduction	0.9196	-0.142	0.8510
Expanding mitered elbow, 30% reduction	3.4955	-0.130	0.9209
Expanding mitered elbow, 50% reduction	29.3450	-0.108	0.9106

Limitations of Results

While the results can be used for engineering purposes, the following limitations should be considered:

1. The dimensions of mitered elbows presented in this research are based off of ANSI/AWWA C208-17 recommendations. Specifically, each miter should not exceed 22.5 degrees and the R/D ratio is 2.5.
2. The reducing and expanding mitered elbows presented in this research are limited to two pipe diameter sizes with reductions of 10%, 30%, and 50%. Although the data showed strong correlations, interpolating the data for different reduction percentages and pipe diameters is discouraged.
3. The *K*s for reducing and expanding mitered elbows must be used with the correct pipe velocity. The *K*s in this research are associated with the slower pipe velocity.
4. One concept that this research did not address is the additional pressure loss that is associated with swirls that extend far beyond downstream from an elbow. The

swirls' turbulence is not accounted for because pipe friction assumes approximately uniform flow conditions.

5. *K*s presented in this research do not include additional lengths on the inlet and outlet sides of the elbow that may be needed to fit field conditions.
6. The *K*s in this research are representative of steel pipe. Pipes of different materials and roughness will vary the pressure losses in any pipe fitting.
7. The physical tests and CFD comparison tests showed an error of ±13.6%.
8. The GCI method used for the CFD's mesh quality showed a numerical error of ±2.6%.
9. Although Star-CCM+ is a great tool for CFD applications, there are several limitations within the software. It is important to understand that the Rκ-ε and Sκ-ε models are attempts to solve the Reynolds-Averaged Navier-Stokes equations, but they are not perfect. For example, the models do not properly adjust the velocity profiles for different pipe diameters. Velocity profiles for smaller pipe diameters should be more parabolic than velocity profiles for much larger pipe diameters. Star-CCM+, however, does not account for this, but rather develops similar velocity profiles for all pipe size diameters. This may create discrepancy between CFD simulations and actual physical data. For example, the results presented in this research for large mitered elbows suggests a strong correlation between *K* and Reynolds number. When graphing Dent's physical data, as shown in Figure 14, the correlation is not as strong. Dent's data, however, does suggest that the correlation of *K* and Reynolds number becomes stronger as pipe size

diameter increases. With the much larger pipe diameters tested in this research, the correlation between *K*, Reynolds number, and different pipe diameter sizes may converge to one relationship if it were to be physically tested in a lab.

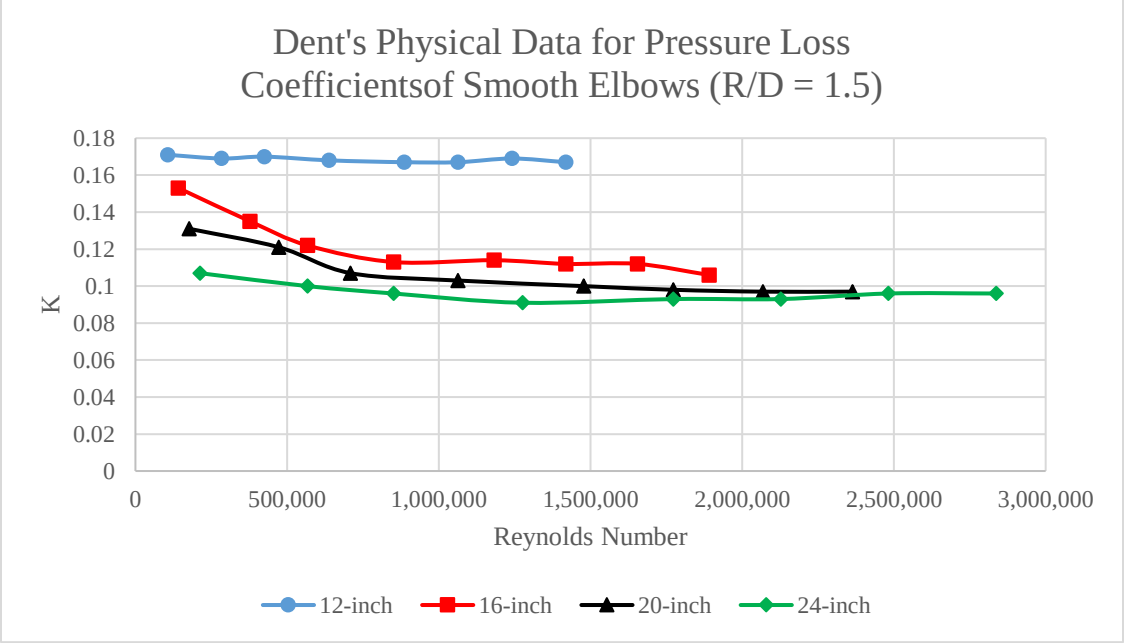

Figure 14. Dent's physical data of pressure loss coefficients for smooth elbows.

10. Although conservative practices were used for the CFD methods in this study, practical engineering thinking is encouraged.

CHAPTER VII

CONCLUSION

There is an extensive amount of research available to predict pressure losses associated with many types of pressure fittings. However, there is little to no data available for pressure losses of larger pipe diameter mitered elbows. The purpose of this research was to investigate pressure loss for large mitered elbows and correlate any relationships with respect to Reynolds number.

Over 350 CFD simulations were made using Star CCM+ software at the UWRL in Logan, Utah to *K* for mitered elbows with 36-inch, 48-inch, 72-inch, 96-inch, and 144-inch pipe diameters. The mitered elbows consisted of 22.5 degree deflections with total bends ranging from 22.5 degrees, 45 degrees, 67.5 degrees, and 90 degrees. *K*s were also produced for reducing and expanding mitered 90 degree elbows with 60 x 54-inch, 60 x 42-inch, 60 x 30-inch, 120 x 108-inch, 120 x 84-inch pipe diameters.

The data suggested that *K* for mitered elbows are solely dependent on Reynolds, and they are additive with respect to the number of 22.5 degree miters in the elbow. Equation 8 is presented to provide an easy method to predict the pressure loss in mitered elbows with relatively minimal error.

Need for Further Research

All mitered elbows in this research had R/D ratios equal to 2.5. Idelchick, Miller, and others have concluded that pressure loss coefficients for elbows are dependent on the elbow's R/D ratio. It is encouraged that additional research be conducted for large

mitered elbows with a variety of R/D ratios. If conducted, it is likely that Equation 8 may be enhanced to predict pressure loss coefficients with any pipe diameter, any number of 22.5 deflections, and any R/D ratio. To achieve this, Equation 8's coefficients would likely become a function of R/D ratios.

The CFD results for reducing and expanding mitered elbows did not provide a strong enough correlation to suggest that *K* is solely dependent on Reynolds number. Only two pipe diameter sizes (60-inch and 120-inch) were investigated with 10%, 30%, and 50% reductions. Additional research is needed to provide more insight on *K* correlations with respect to pipe diameter, percentage of reduction, and Reynolds number.

Due to the limitations of Star-CCM+, there may be discrepancies between CFD simulations and physical data, as mentioned in the limitations section of this thesis. While it may not be feasible to conduct physical testing of mitered elbows with the large diameters in this research, it would still be beneficial to conduct physical testing of similar mitered elbows with diameters ranging from 24-inches to as large as feasibly possible. These physical tests of these mitered elbows would provide additional insight to the correlation of pressure loss coefficients and Reynolds number.

REFERENCES

AWWA (American Water Works Association). (2017). *Quarter-Turn Valves: Head Loss, Torque, and Cavitation Analysis*, 3rd Edition. Manual of Water Supply Practices, M49. AWWA, Denver.

AWWA. (2017). *AWWA Standard for Dimensions for Fabricated Steel Water Pipe Fittings*. ANSI/AWWA C208-17. AWWA, Denver.

CD-adapco. (2018). "STAR-CCM+ User Guide Version 13.04." <https://mdx.plm.automation.siemens.com/star-ccm-plus> (Jan. 11, 2018).

Celik, I.B., Ghia, U., Roache, P.J., Freitas, C.J., Coleman, H., Raad, P.E. (2008). "Procedure for Estimation and Reporting of Uncertainty Due to Discretization in CFD Applications." *Journal of Fluids Engineering-Transactions of the American Society of Mechanical Engineers*, 130:078001-3.

Crane. (2010). *Flow of Fluids Through Valves, Fittings, and Pipe. Crane Co. Technical paper No. 410*. Crane Company. Joilet, Ill.

Dent, P. (2000). "Develop Design Data on Pressure Loss of Large Pipe Fittings." M.S. thesis, Utah State Univ., Logan, Utah.

Ding, C., Carlson, L., Ellis, C.R., Mohseni, O. (2005). "Pressure Loss Coefficients of 6, 8 and 10-inch Steel Pipe Fittings." St. Anthony Falls Laboratory. *American Society of Heating, Refrigerating and Air-Conditioning Engineers, Inc.*, Research project No. 1116-TRP. Retrieved from the University of Minnesota Digital Conservancy, <http://hdl.handle.net/11299/113368.> (Oct. 18, 2017)

Idelchik, I.E. (2008). (3rd ed.). *Handbook of Hydraulic Resistance*, 3rd Edition. Research Institute for Gass Purification (M.O. Steinverg, editor). Jaico Publishing House, Mumbai.

ISO (Internation Organization for Standardization). (1991). *Measurement of Fluid Flow by Means of Pressure Differential Devies – Part 1: Orifice Plates, Nozzles, and Venturi Tubes Inserted in Circular Cross-Section Conduits Running Full.* ISO 5167-1:1999, ISO. Geneva.

Koch, P. (2006). "The influence of Reynolds Number and size effects on pressure loss factors of ductwork components." *Building Services Engineering Research and Technology*, 27,4 (2006) pp. 261-283.

Miller, D.S. (2011). *Internal Flow Systems*. Miller Innovations, Bedford, UK.

Moujaes, S.F., Deshmukh, S. (2006). “Three-Dimensional CFD Predications and Experimental Comparison of Pressure Drop of Some Common Pipe Fittings in Turbulent Flow.” *Journal of Energy Engineering,* ASCE. DOI: 10.1061/(ASCE)0733-9402(206) 132:2(61).

Rahmeyer, W. J. (1999). “Pressure Loss Coefficients for Threaded and Forged Weld Pipe Ells, Reducing Ells, and Pipe Reducers.” *American Society of Heating, Refrigerating and Air-Conditioning Engineers, Inc. Transactions,* 105(2):334-354.

APPENDICES

Appendix A – CFD simulations for a 72-inch diameter mitered elbow (R/D = 2.5) operating at a velocity of 12 feet per second

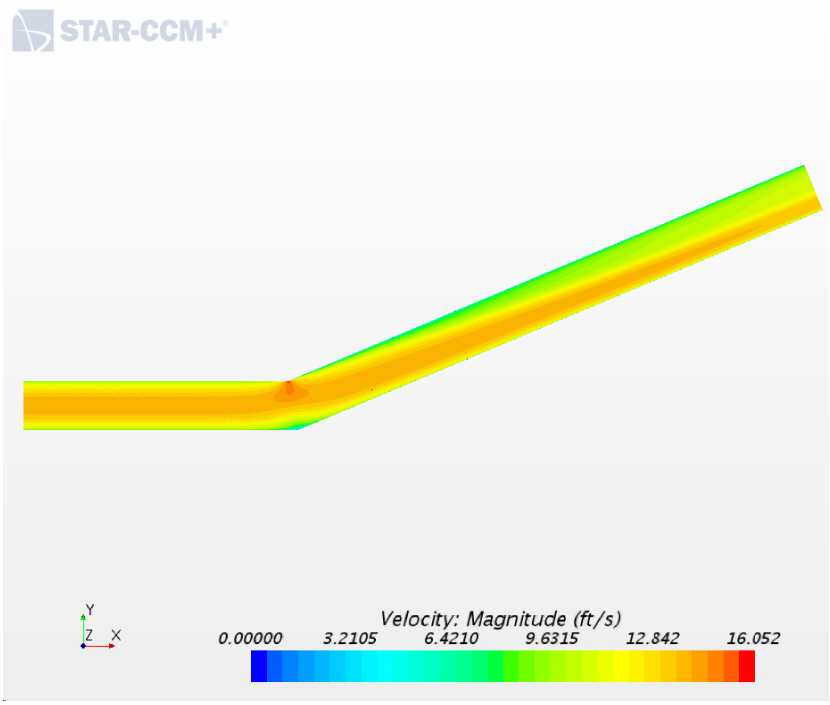

Figure 15. 72-inch diameter mitered elbow with total deflection of 22.5 degrees

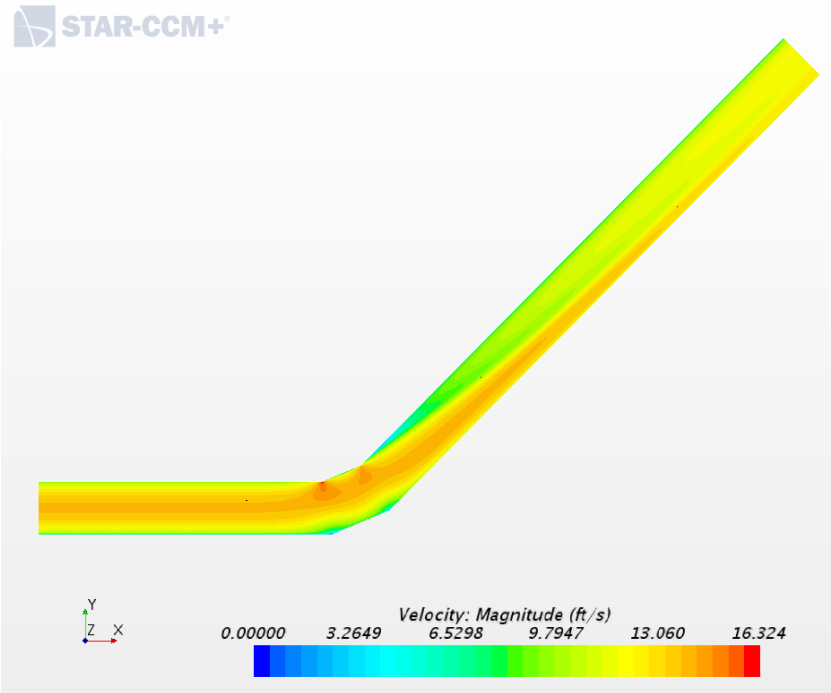

Figure 16. 72-inch diameter mitered elbow with total deflection of 45 degrees

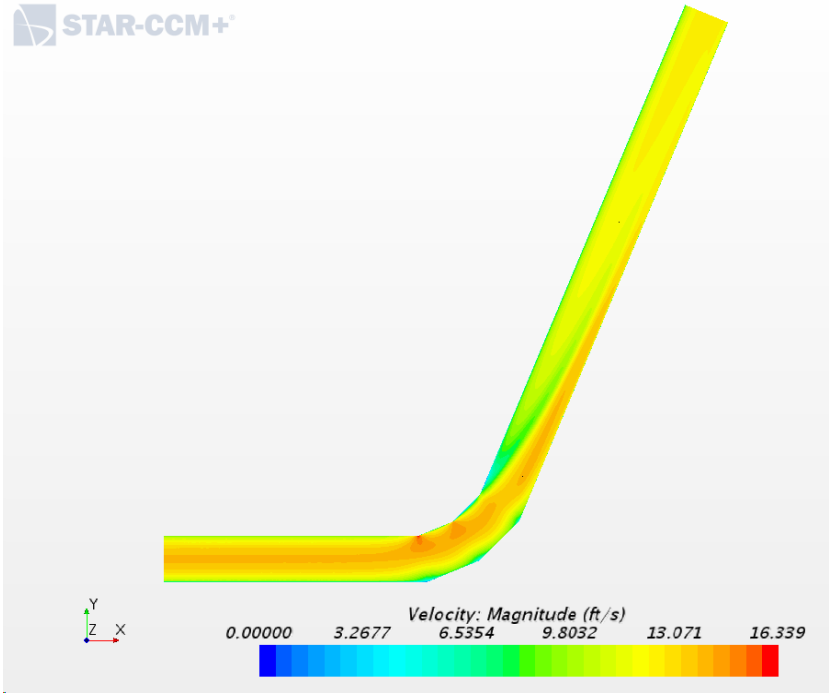

Figure 17. 72-inch diameter mitered elbow with total deflection of 67.5 degrees

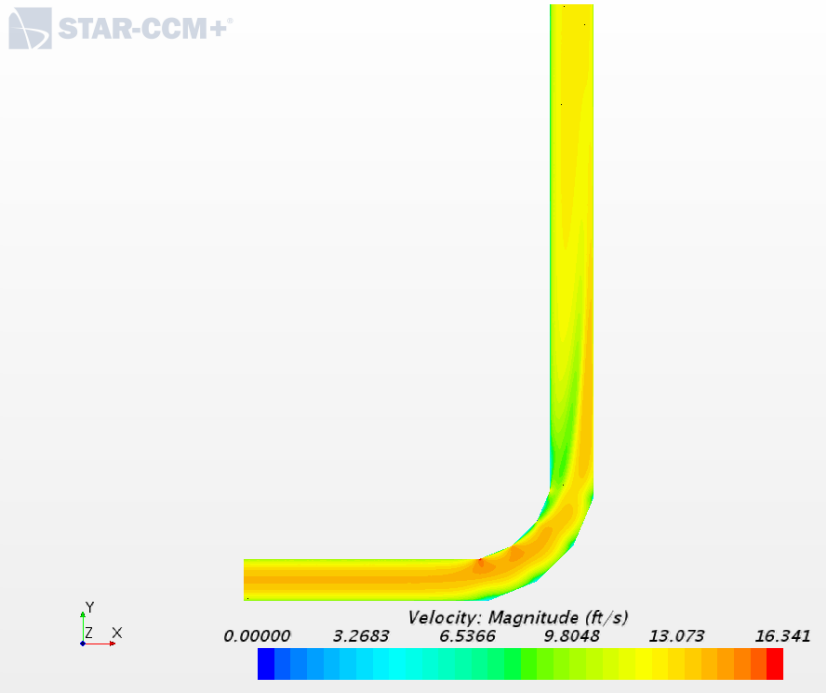

Figure 18. 72-inch diameter mitered elbow with total deflection of 90 degrees

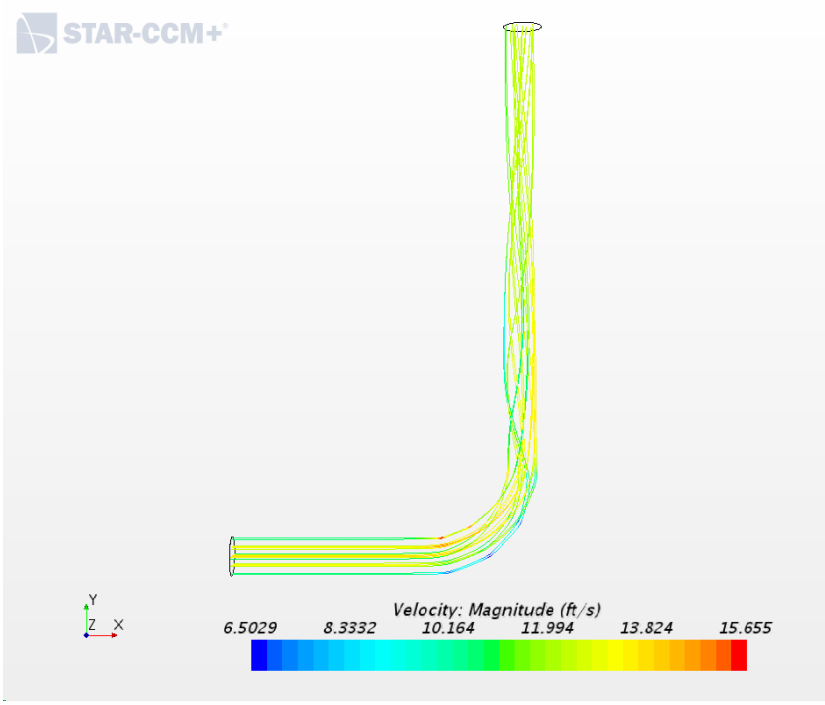

Figure 19. Plan view of streamlines through a 72-inch diameter 90 degree mitered elbow

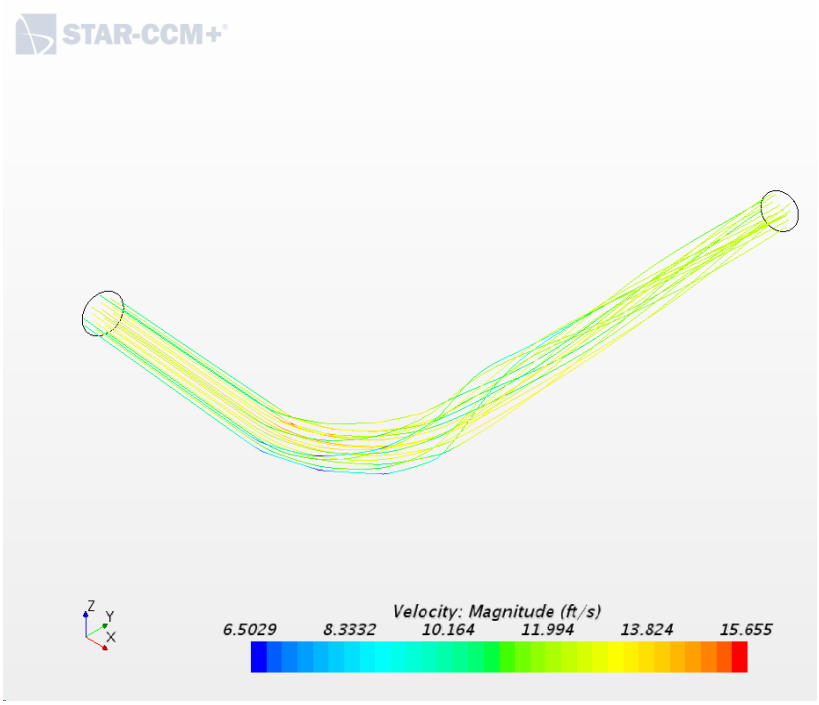

Figure 20. Isometric view of streamlines through a 72-inch diameter 90 degree mitered elbow

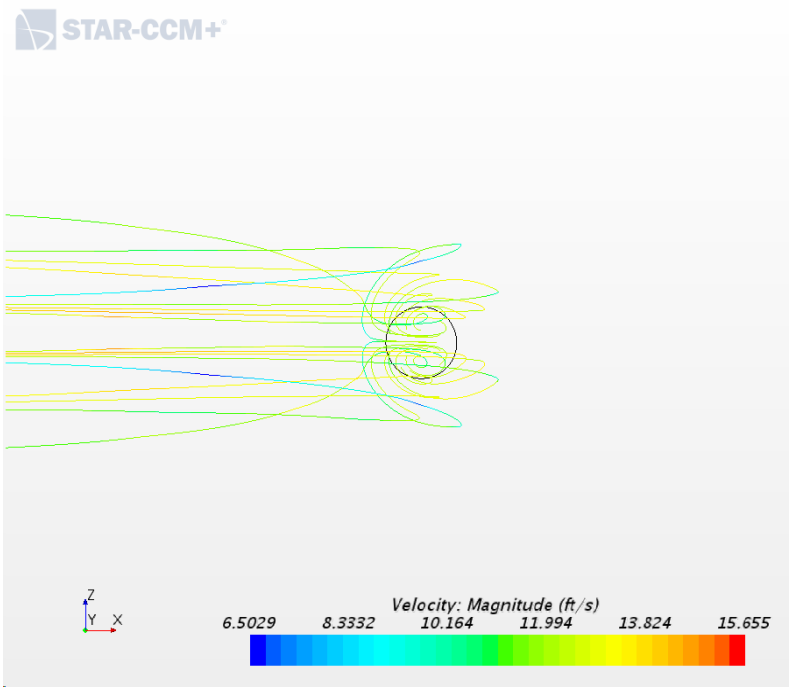

Figure 21. Cross-sectional view of streamlines through a 72-inch diameter 90 degree mitered elbow

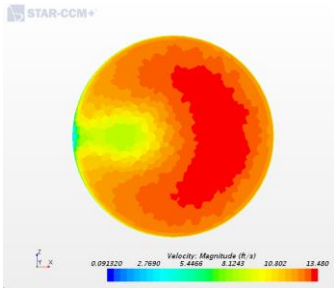

A. Cross-section located directly downstream from elbow

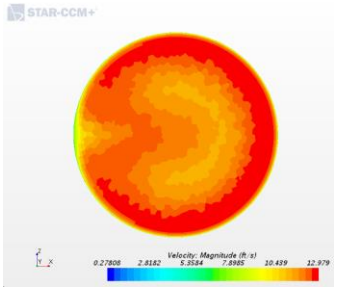

B. Cross-section located five diameters downstream from elbow

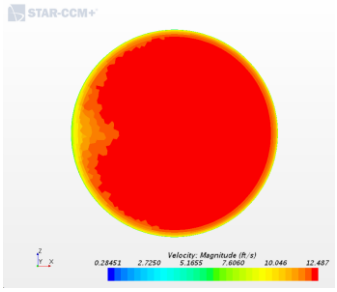

C. Cross-section located ten diameters downstream from elbow

Figure 22. Velocity profiles downstream from a 72-inch diameter 90 degree mitered elbow

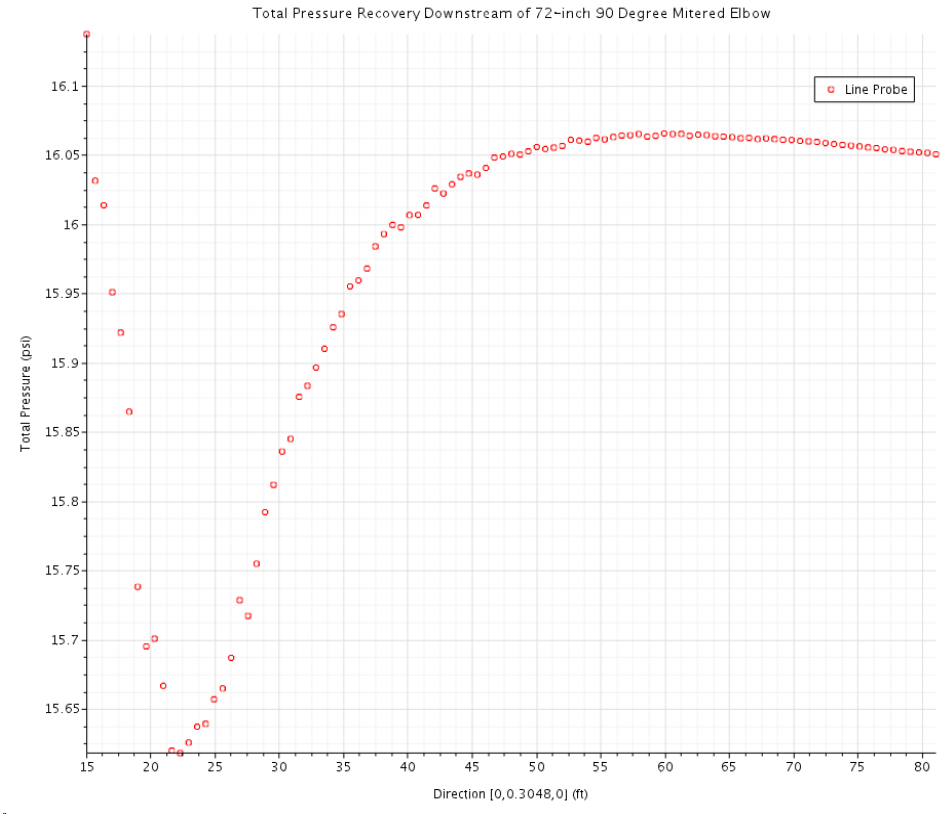

Figure 23. Example of total pressure recovery of a 72-inch diameter 90 degree mitered elbow

Appendix B – CFD simulations for reducing mitered elbows (R/D = 2.5) with upstream velocities operating 12 feet per second

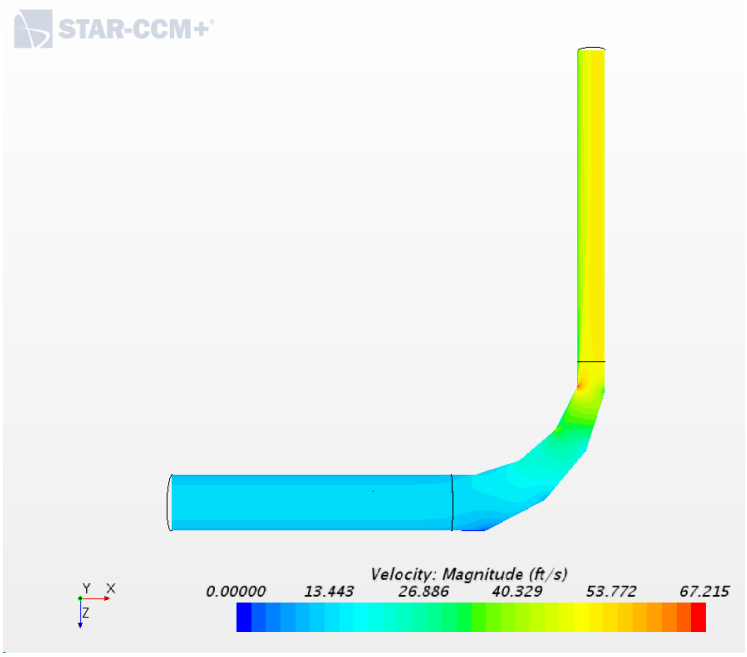

Figure 24. 60 x 30-inch 90 degree reducing mitered elbow

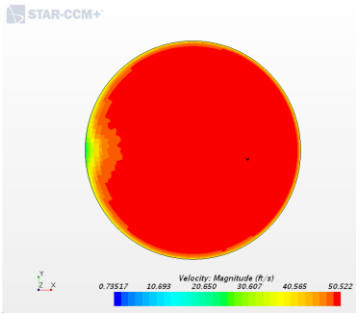

A. Cross-section located directly downstream from elbow

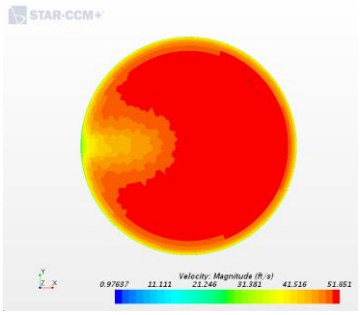

B. Cross-section located five diameters downstream from elbow

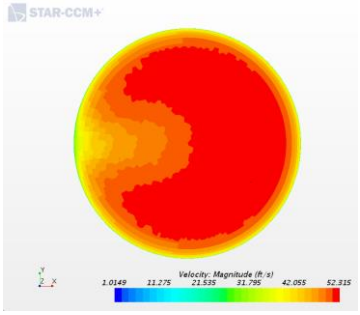

C. Cross-section located ten diameters downstream from elbow

Figure 25. Velocity profiles downstream from a 60 x 30-inch 90 degree reducing mitered elbow

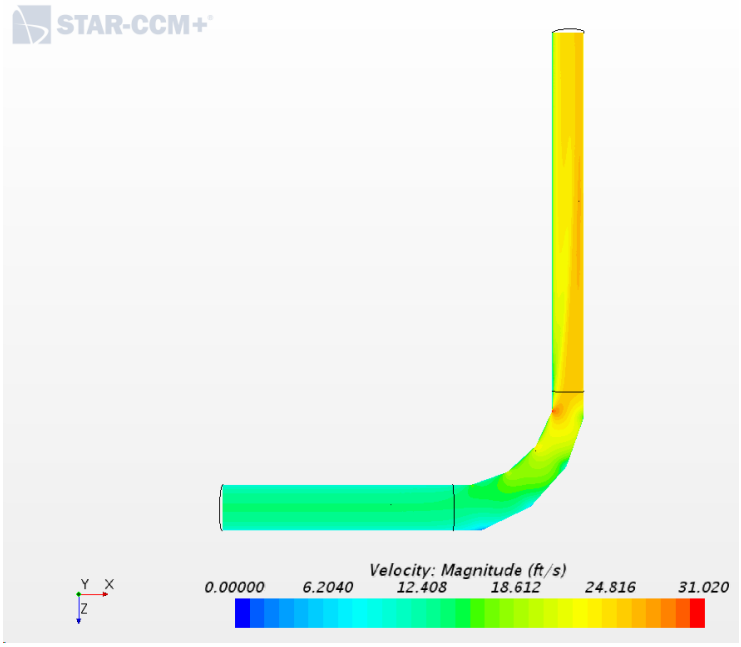

Figure 26. 60 x 42-inch 90 degree reducing mitered elbow

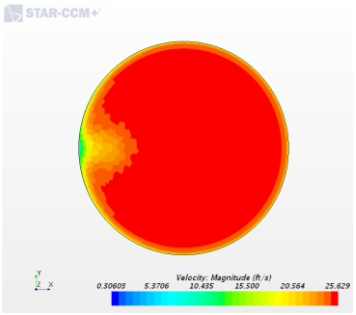

A. Cross-section located directly downstream from elbow

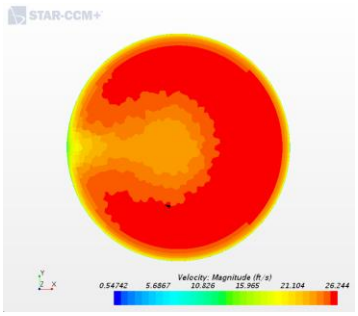

B. Cross-section located five diameters downstream from elbow

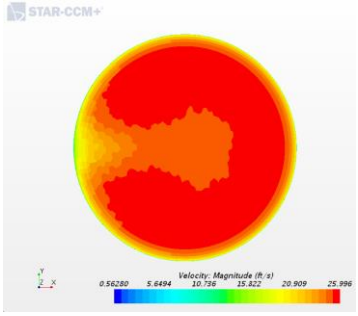

C. Cross-section located ten diameters downstream from elbow

Figure 27. Velocity profiles downstream from a 60 x 42-inch 90 degree reducing mitered elbow

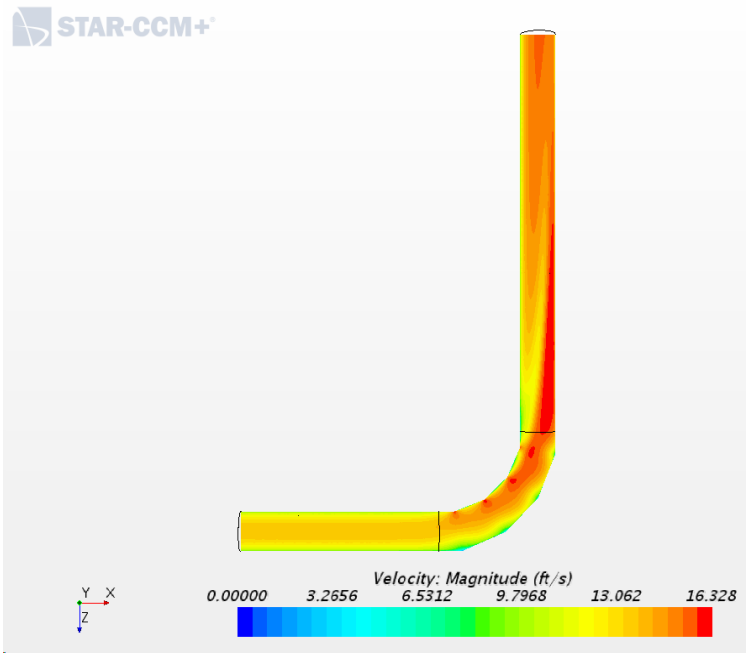

Figure 28. 60 x 54-inch 90 degree reducing mitered elbow

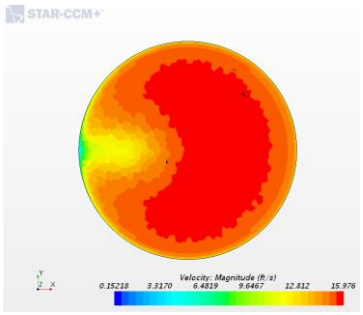

A. Cross-section located directly downstream from elbow

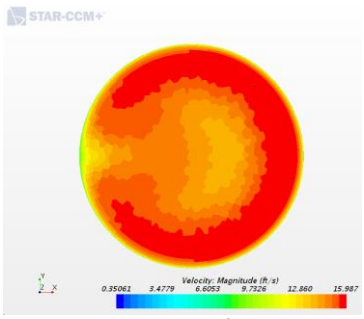

B. Cross-section located five diameters downstream from elbow

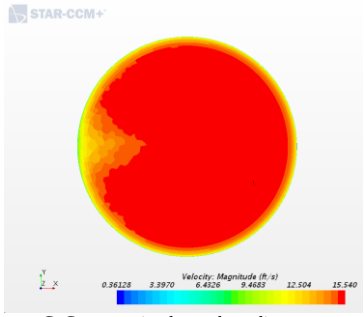

C. Cross-section located ten diameters downstream from elbow

Figure 29. Velocity profiles downstream from a 60 x 54-inch 90 degree reducing mitered elbow

Appendix C – CFD simulations for expanding mitered elbows (R/D = 2.5) with downstream velocities operating 12 feet per second

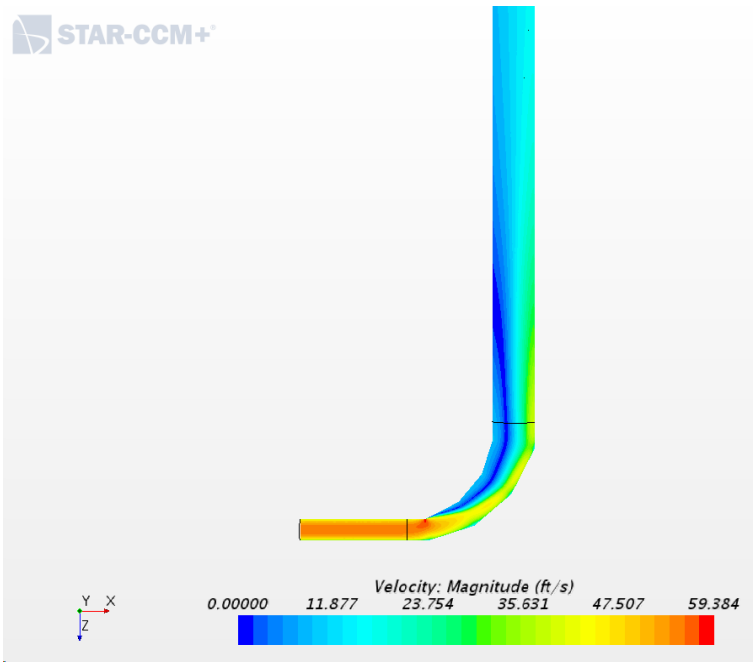

Figure 30. 30 x 60-inch 90 degree expanding mitered elbow

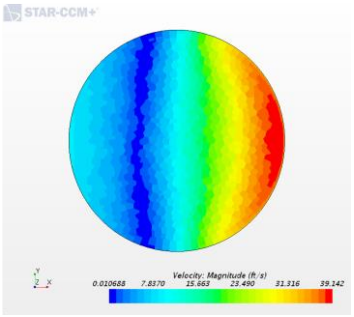

A. Cross-section located directly downstream from elbow

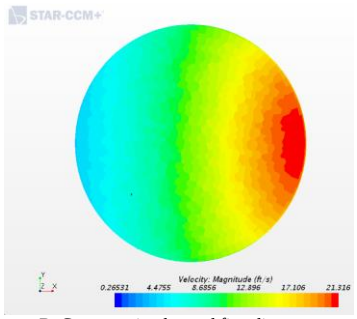

B. Cross-section located five diameters downstream from elbow

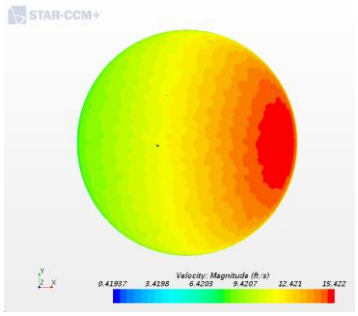

C. Cross-section located ten diameters downstream from elbow

Figure 31. Velocity profiles downstream from a 30 x 60-inch 90 degree expanding mitered elbow

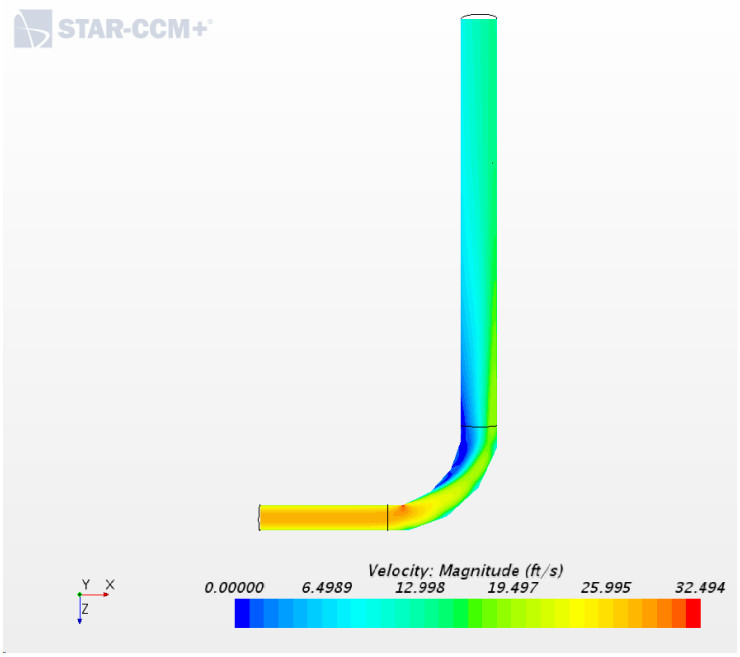

Figure 32. 42 x 60-inch 90 degree expanding mitered elbow

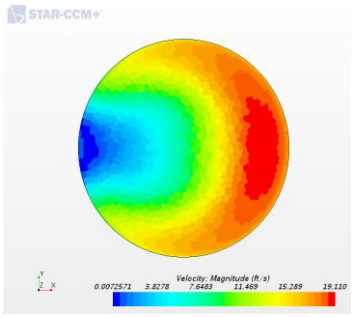

A. Cross-section located directly downstream from elbow

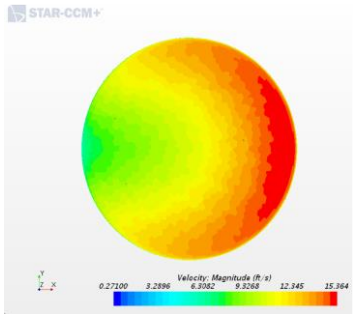

B. Cross-section located five diameters downstream from elbow

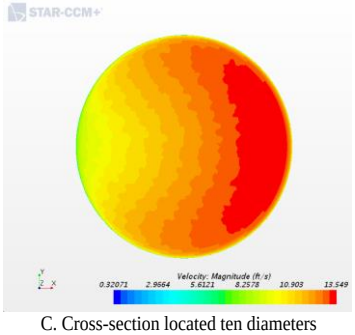

C. Cross-section located ten diameters downstream from elbow

Figure 33. Velocity profiles downstream from a 42 x 60-inch 90 degree expanding mitered elbow

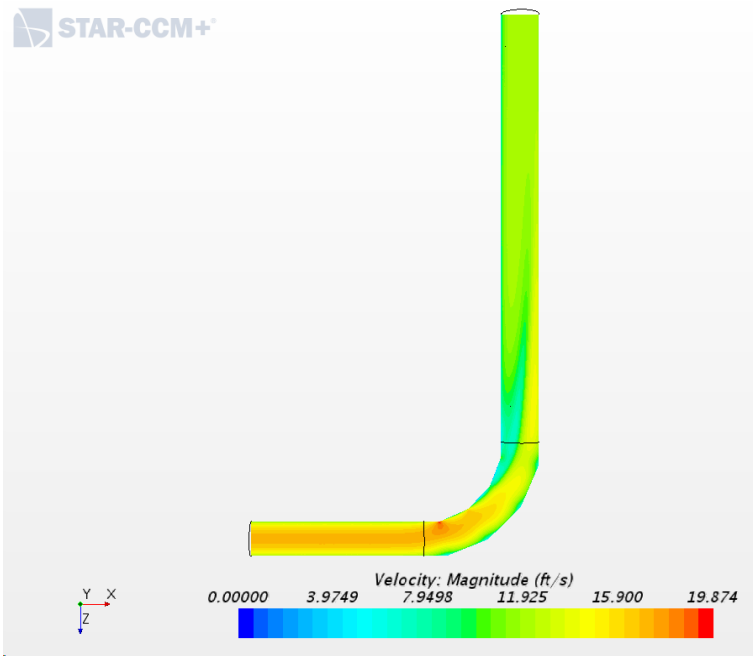

Figure 34. 54 x 60-inch 90 degree expanding mitered elbow

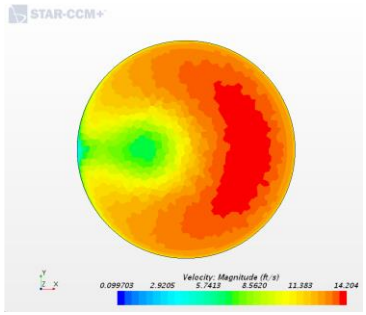

A. Cross-section located directly downstream from elbow

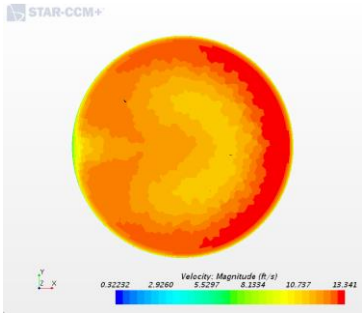

B. Cross-section located five diameters downstream from elbow

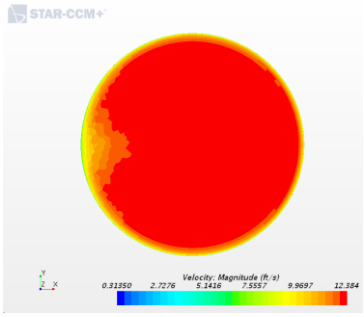

C. Cross-section located ten diameters downstream from elbow

Figure 35. Velocity profiles downstream from a 54 x 60-inch 90 degree expanding mitered elbow